# Sensitivity of a Sahelian groundwater-based agroforestry system to tree density and water availability using the land surface model ORCHIDEE (r7949)

Espoir Koudjo Gaglo[1,2], Emeline Chaste[5], Sebastiaan Luyssaert[7], Olivier Roupsard[2,4,5], Christophe Jourdan[5], Sidy Sow[2,3], Nadeige Vandewalle[8,9], Frédéric Do[2,5,6], Daouda Ngom[1], Aude Valade[5]

[1]Université Cheikh Anta Diop, Dakar, Senegal
[2]LMI IESOL, IRD, ISRA, Bel Air, Dakar, Senegal
[3]Université Gaston Berger, Saint-Louis, Senegal
[4]CIRAD, UMR Eco&Sols, Dakar, Senegal
[5]Eco&Sols, University Montpellier, CIRAD, INRAE, Institut Agro, IRD, Montpellier, France
[6]IRD, UMR Eco & Sols, Univ Montpellier, IRD, CIRAD, INRAE, Montpellier, France
[7]A-LIFE, Vrije Universiteit Amsterdam, Amsterdam, Netherlands
[8]Earth and Life Institute, Faculty of Bioscience Engineering, Catholic University of Louvain, Louvain-la-Neuve, Belgium
[9]Terra Teaching and Research Center, University of Liège, Gembloux Agro-Bio Tech, Gembloux, Belgium

*Correspondence:* Espoir Koudjo Gaglo, (espoirkoudjo.gaglo@ucad.edu.sn)

**Abstract.** The Sahel region is characterized by its semi-arid climate and open-canopy agroforestry systems which play an important role in global carbon dynamics by sequestering an estimated 0.4 Mg C ha$^{-1}$ yr$^{-1}$, contributing to a total potential sequestration of approximately 558 Tg C if the agroforestry systems reach their maximum extent. However, land surface models (LSM) used in global climate modeling struggle to represent carbon dynamics in these ecosystems due to the inadequate representation of deep-roots tapping groundwater during dry periods, key environmental control for many agroforestry systems such as the widespread parklands based on the phreatophytic species *Faidherbia albida*. This study explores the sensitivity of *Faidherbia albida* parklands to tree density and water availability (rainfall and soil water content in the capillary fringe of the groundwater table) using a new configuration of the ORCHIDEE LSM. To this aim, the ORCHIDEE LSM was modified to simulate the growth of *Faidherbia albida* by simulating its inverted phenology based on forced temporal series of soil water content of soil layers between 4 m and 5 m and water saturation below 5 m and by adjusting the photosynthesis and carbon allocation parameters for *Faidherbia albida* and associated crops. The model was evaluated against independent eddy covariance and meteorological data from the Niakhar agroforestry site in Senegal. Simulation outputs were analyzed in terms of leaf area index (LAI), gross primary productivity (GPP), latent heat (LE), sensible heat (H) and net radiation (Rn). The model simulated tree GPP of 4.08 ± 0.21 tC ha$^{-1}$ yr$^{-1}$ compared to observed GPP of 5.06 ± 0.49 tC ha$^{-1}$ yr$^{-1}$. For croplands, the model produced GPP of 7.97 ± 0.89 tC ha$^{-1}$ yr$^{-1}$ compared to observed values of 7.78 ± 1.75 tC ha$^{-1}$ yr$^{-1}$. Simulations revealed that tree density positively influenced annual carbon uptake but reduced crop harvest at highest tree densities, indicating a trade-off between carbon sequestration and crop yield. Sensitivity analyses showed that interannual variability in soil water content in the capillary fringe of the groundwater table and rainfall influenced differently crop, tree

and ecosystem carbon and energy fluxes. Despite its strengths, the model exhibited limited responsiveness of tree productivity

35 to soil water content variability in the capillary fringe of the groundwater table, highlighting the need for enhanced representation of water uptake by tree roots in the model. These findings emphasize the importance of accurately modeling both surface soil water and groundwater dynamics and phenology to predict the responses of semi-arid agroforestry systems to climate variability. This study enhances our understanding of carbon and energy flux partitioning in complex, water-stressed and groundwater dependent agroforestry systems.

40 Keywords: Sahelian agroforestry, *Faidherbia albida*, groundwater-dependent ecosystems, Land Surface Model.


**1 Introduction**

Although rainfall has long been recognized as the primary factor influencing vegetation distribution in the West African Sahel (Ndehedehe et al., 2019; Seghieri et al., 2009), analyses of 12-year time series of correlations between normalized difference vegetation index and water availability (Ndehedehe et al., 2016) have shown that terrestrial water storage serves as an

45 additional driver of vegetation dynamics (Ndehedehe et al., 2019). Many Sahelian plants rely on deep root systems that access groundwater at depths of up to 40 meters (Antunes et al., 2018; Do et al., 2005), providing an important water source in arid landscapes (Huber et al., 2011). The reliance on both rainfall and groundwater is essential for vegetation resilience and contributes to the observed increase in vegetation cover in nearly 24 % of the Western and Central Sahel since the 1980s, a process now commonly referred to as "Sahel regreening" (Dardel et al., 2014; Fensholt et al., 2013; Herrmann et al., 2005).

50 While regreening is largely driven by rainfall, human-induced changes in land use also play an important role. Agricultural practices, such as land clearing and the adoption of specific cropping systems, have altered soil properties, reduced transpiration, and increased surface runoff, which, in turn, has enhanced groundwater recharge (Charreau and Fauck, 1970; Scanlon et al., 2005, 2006). Groundwater levels in some areas of the Sahel have risen, even during periods of declining rainfall, such as the severe droughts of the 1970s and 1980s (Descroix et al., 2009; Favreau et al., 2009), highlighting the resilience of

55 the Sahel region's hydrological systems (Leduc et al., 2001). Projections under future climate scenarios, however, suggest a decrease in West African rainfall, particularly in the western portion of it, with increasing severity at higher global warming levels (Dosio et al., 2021; Kumi and Abiodun, 2018) potentially challenging this resilience. Such projected decrease in rainfall could indeed lead to a decline in groundwater recharge and storage (Kotchoni et al., 2019; Toure et al., 2016), threatening the sustainability of both vegetation and water resources (Glanville et al., 2023; Yin et al., 2015).

60 *Faidherbia albida* parklands are agroforestry systems commonly found in the Sahelian landscape. These agroforestry systems are widespread due to the natural distribution of *Faidherbia albida* trees across a broad geographic area from Senegal to Ethiopia, including parts of Southern Africa (Barnes and Fagg, 2003; Maslin et al., 2003; Vandenbeldt et al., 1992; Wickens, 1969). *Faidherbia albida* parklands are a specific type of agroforestry system relying mainly on groundwater dynamics thanks to the phreatophyte behavior of *Faidherbia albida* trees (Barnes and Fagg, 2003; Roupsard et al., 1999). The trees' taproots

65    can extend down to 20 meters to access groundwater and extract nutrients from deeper soil layers, which it cycles back to the surface soil layers (Barnes and Fagg, 2003; Sileshi, 2016). In magnitude, the water use of *Faidherbia albida* trees at the plot scale was estimated to be less than 10 % of the annual amount of rainfall (Roupsard et al., 1999; Sarr et al., 2023). However, stable isotope tracing suggested a strong dependence of tree water use on groundwater (Roupsard et al., 1999). In environments where the groundwater is relatively shallow, *Faidherbia albida* was reported to have a bimodal root distribution, with a high

70    density of fine roots in the shallow soil (30-60 cm), allowing the capture of surface nutrients, and an increase in root density near the groundwater, which allows for the extraction of groundwater from the capillary fringe (Gning et al., 2023; Roupsard et al., 1999; Siegwart et al., 2023). *Faidherbia albida* is also characterized by a peculiar reverse phenology, as its leaves typically develop during the dry season but shed during the rainy season. A strong benefit of the reverse phenology for farms is that trees can be pruned throughout the dry season for feeding cattle, and leaves and pods provide valuable forage for

75    livestock during the dry season when other feed sources are scarce (Barnes and Fagg, 2003). This reverse phenology also reduces competition for water and light between trees and crops during the wet season and an increase in crop yield in the vicinity of trees was reported (Roupsard et al., 2020).

Land Surface Models (LSMs) describe biophysical processes within the soil-plant-atmosphere continuum at scales ranging from plots to the globe (Boucher et al., 2020; Lawrence et al., 2019). At the global scale, LSMs serve as the land surface

80    components of Earth System Models, which are used by organizations such as the Intergovernmental Panel on Climate Change for climate projections (Meinshausen et al., 2024). Substantial uncertainties in simulating dryland ecosystems by current LSMs have been documented (Fawcett et al., 2022). These uncertainties underscore the need for model refinements and caution when interpreting LSM estimates of carbon dynamics in semi-arid regions such as the Sahel. In particular, LSMs often fail to adequately represent deep-rooted plants that access groundwater during dry periods (Bastos et al., 2022; MacBean et al., 2021).

85    The ORCHIDEE model is the land surface component of the Institut Pierre Simon Laplace — Earth System Model (Boucher et al., 2020; Krinner et al., 2005). ORCHIDEE is a global process-based terrestrial biosphere model that calculates the fluxes of carbon, nitrogen, water, and energy between the surface and the atmosphere (Krinner et al., 2005). ORCHIDEE can be coupled with a global climate model to allow the analysis of vegetation feedback and land use on the climate, or be used as a standalone model as in this study, forced by climate data, to assess the impact of climate on ecosystems, among other

90    applications (Boucher et al., 2020).

Considering the beneficial effects of *Faidherbia albida* and their importance for Sahel as well as the uncertainty in the response of semi-arid ecosystems to future global warming, this study raises the question of the sensitivity of *Faidherbia albida* parklands to tree density and water (rain and water in the capillary fringe of the groundwater) availability. To address this question, the LSM ORCHIDEE (revision 7949) was specifically configured for *Faidherbia albida* to assess how tree density

95    and water availability influence carbon and energy fluxes in dryland ecosystems. As a first approach on mature *Faidherbia*

*albida* trees, this development of ORCHIDEE assumed a permanent phreatophyte type relying only on the groundwater for water uptake and as a driver for phenology.

The objectives of this study are: (1) to evaluate the skills of the newly configured version of ORCHIDEE by comparing its simulations with independent data on the *Faidherbia albida* ecosystem, (2) to assess the sensitivity of tree and crop

100 productivity, as well as energy and carbon fluxes, to variations in tree density and water availability.

## 2 Materials and methods

### 2.1 Study area

The study was conducted in the actively farmed agroforestry parkland of Niakhar, in the agricultural zone classified as the "groundnut basin" of Senegal, Western Africa (Fatick region, 135 km east of Dakar) (Figure 1). The climate of Niakhar is

105 Sudano-Sahelian, with a wet season ranging from June to October and a dry season ranging from November to May. Niakhar is an area of dynamic agro-silvo-pastoral fields dominated by the multifunctional tree *Faidherbia albida*. The main crops are pearl millet and groundnut, conducted in annual rotation. *Faidherbia albida* trees are spread across the landscape at a density of 13 trees ha$^{-1}$ in the study area just around the eddy covariance tower, equivalent to a canopy cover of 15 % as calculated from the average crown area of 116 m² per tree. Based on surveys of 3000 trees in Niakhar (Lalou R., Montes N., pers. comm.),

110 and dendrochronology analysis (Dougabka D., pers. comm.), the average age of the *Faidherbia albida* trees in this site was estimated at 55 years, the average tree diameter and height were 0.67 m and 12.8 m, respectively.
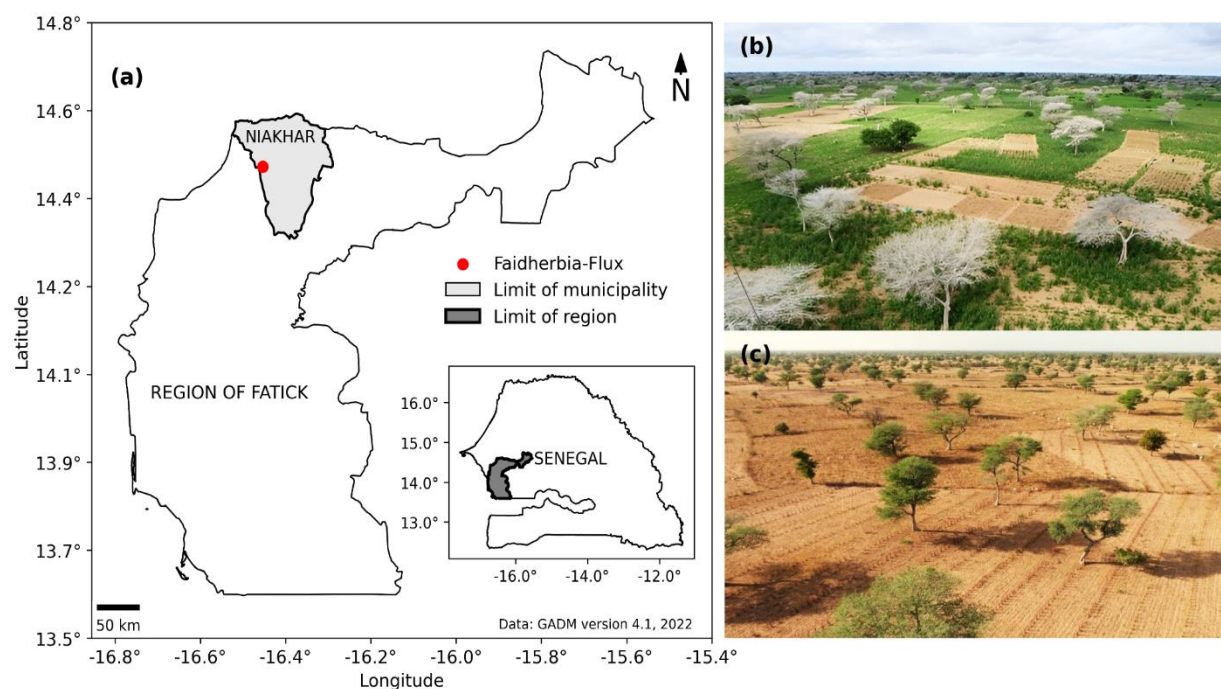
**Figure 1: (a) Location of the Faidherbia-Flux observatory (Niakhar, Senegal). Pictures of the agro-silvo-pastoral ecosystem dominated by the reverse phenology *Faidherbia albida* trees in Niakhar during the (b) wet (trees are defoliated, crops are growing)**
115 **and (c) dry seasons (trees are in leaf, the soil is bare). Photos: Olivier Roupsard**

## 2.2 Faidherbia-Flux measurement setup

The data used in this study originate from the experimental site "Faidherbia-Flux", located at N: 14°29′44.916″; W: 16°27′12.851″ (Roupsard et al., 2020). The Faidherbia-flux database holds half-hourly flux estimates from eddy covariance measurements and the associated weather and ancillary variables.

120 **2.2.1 Eddy covariance flux, climate variables and leaf area index**

Half-hourly data of the "Faidherbia-Flux" site from 2018 to 2023 were extracted from the database. The eddy-covariance system (Li-COR SMARTFLUX including a Gill MasterPro 3D sonic anemometer and a LI-7500 RS open path $CO_2$ and $H_2O$ gas analyzer) was mounted at 20 m high on a 30 m high mast and monitored the ecosystem exchange of sensible heat (H), latent heat (LE), and $CO_2$ above the agroforestry system including trees, crops, and soil. Climate variables measured at 20 m
125 high include air temperature and relative humidity (also measured at 2 m high), wind speed, atmospheric pressure, and rainfall by making use of the CS215 Campbell, the WindSonic 4 Campbell, the SMARTFLUX, and the Texas Electronics model TE525MM instruments, respectively. Net radiation was measured at 20 m by a nRlite net radiometer (Kipp & Zonen).

5

The eddy-covariance raw data were acquired at a frequency of 20 Hz using SMARTFLUX and post-processed using the advanced mode of the EddyPro v7.0 software by making use of the SMARTFLUX '.ghg' files. The following options were

130 used in EddyPro: (1) raw data processing (automatic angle-of-attack correction for wind components (Gill sonic anemometers), double axis rotation for tilt correction, block average detrend method for turbulent fluctuations, covariance maximization with default for time-lag compensation); (2) compensation for density fluctuations (WPL terms, Webb et al., (1980)); (3) quality checks — flagging policy (Foken et al., 2005); (4) statistical tests for raw data screening following (Vickers and Mahrt, 1997); (5) estimation of random uncertainty due to sampling error (Finkelstein and Sims, 2001); (6) spectra and cospectra calculation

135 and corrections (low-frequency range according to Moncrieff et al., (2005) and high frequency range according to Moncrieff et al., (1997)). Footprints were computed according to Kormann and Meixner, (2001), using the FREddyPro R package (Xenakis, 2016). Gap-filling and partitioning of $CO_2$ data were performed using the ReddyProc R package (Wutzler et al., 2018), selecting the daytime partitioning model of Lasslop et al., (2010).

Tree leaf area density was estimated by optical indirect measurements every ten days at 4 azimuths under 13 trees and above

140 (in a nearby clearing) at the plot scale using the Li-Cor LAI2200, at dawn to have 100 % diffuse light and further analyzed following the 'isolated tree' protocol (Li-Cor, 2012; Taugourdeau et al., 2014). Tree leaf area index (LAI) was computed by multiplying the crown volume by leaf area density and dividing by the projected crown area. Tree LAI was filtered for anomalous data which occur when below and above canopy measurements do not perfectly represent the same sky area and gap-filled using visual estimation of the proportion of leaves in the crowns, monitored every ten days by one single operator.

145 Crop LAI dynamics were derived at the semi-hourly time-step from normalized difference vegetation index measurements using a proxy detection of normalized difference vegetation index sensor placed on the tall mast and directed to the crops (Pontailler et al., 2003), with data filtering according to Soudani et al., (2012) and an annual calibration of normalized difference vegetation index with the actual crop LAI from crop harvest in subplots, according to Diongue et al., (2022) and Roupsard et al., (2020).

150 **2.2.2 Soil measurements**

The dominant soil around Niakhar contains 88.1 ± 4.9 % sand, 6.1 ± 0.6 % silt, and 5.8 ± 1.6 % clay and is poor in organic matter (Diongue et al., 2022; Roupsard et al., 2020). The soil depth is about 8 m limited by the Eocene sandstone bedrock. Soil humidity at nine depths (15, 30, 50, 75, 100, 125, 150, 175, and 200 cm) were recorded with automated time domain reflectometers (CS615, Campbell Scientific, UK) (Diongue et al., 2022). Groundwater fluctuations between 5 and 6 m were

155 recorded with piezometers and revealed a brackish water table at a depth of approximately 6 m (Diongue et al., 2023). The soil water content in the capillary fringe of the groundwater (SWCC) was measured with a time domain reflectometer probe inserted at 4.8 m deep in a well.

### 2.2.3 Photosynthetic parameters (Vcmax and Jmax)

The rubisco activity (Vcmax) and the electron transport rate (Jmax) were measured from A_Ci and A_PAR curves every two
160 weeks for 3 days in a row, in the same tree on sunlit leaves of the top canopy from January to April (Vandewalle, 2024).

### 2.3 ORCHIDEE configuration for *Faidherbia albida* ecosystems

This study makes use of ORCHIDEE revision 7949 which is referred to as the standard configuration of the model in this
study. We adjusted the code of revision 7949 to the *Faidherbia albida* agroforestry systems by modifying the modules for soil,
root, and phenology, and by adjusting the photosynthesis and carbon allocation and assimilation parameters (Figure 2). The
165 modified configuration (Table S1) is referred to as the "Faidherbia configuration".



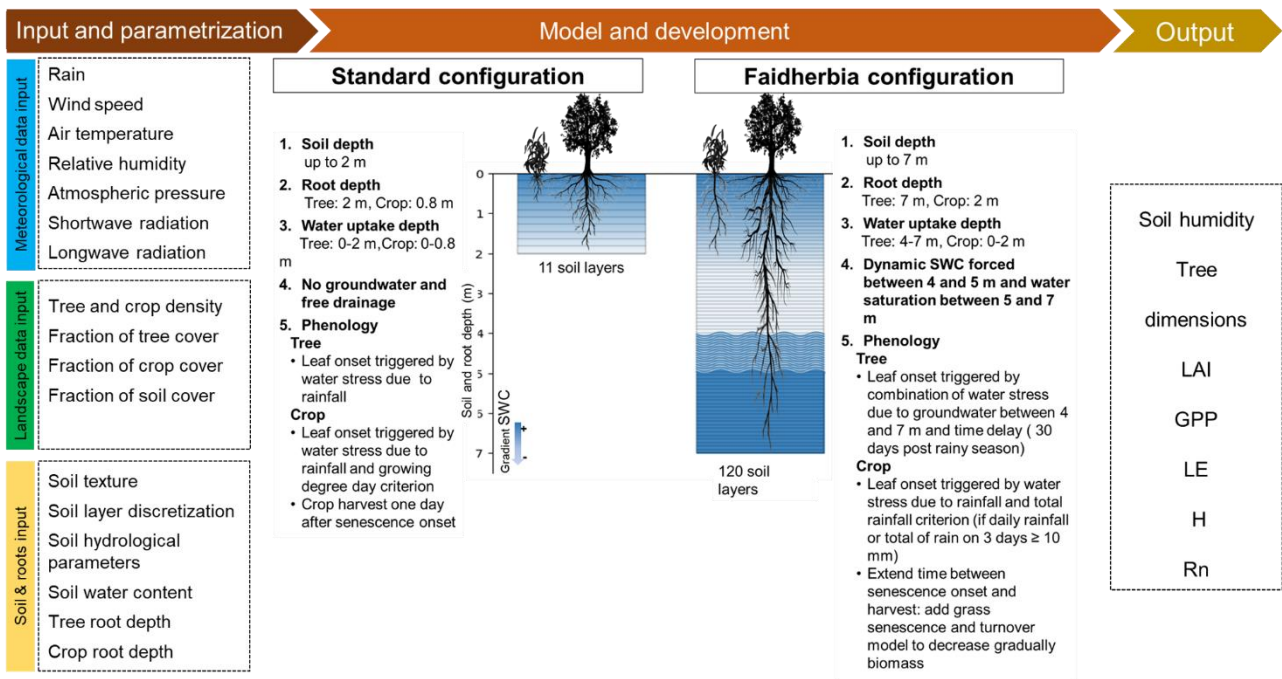**Figure 2: Schematic diagram of the ORCHIDEE standard model and Faidherbia configurations showing the input data required,
the process modifications and a non-exhaustive list of the model output variables used in this study. SWC: soil water content; LAI:
170 leaf area index; GPP: gross primary productivity; LE: latent heat flux; H: sensible heat flux; Rn: net radiation.**

### 2.3.1 Vegetation description

Vegetated areas in the model are defined by up to 14 plant functional types (PFTs) in addition to bare soil. A PFT is characterized by a classification scheme that takes into account physiognomy (tree or grass), leaf morphology (needleleaf or broadleaf), phenology (evergreen, summer-green, or rain-green), photosynthetic pathway (C3 and C4), and climatic zones (boreal, temperate and tropical) (Krinner et al., 2005; Poulter et al., 2015). For this study, three PFTs were used: bare soil, tropical deciduous summer-green trees, and C4 crop with areal cover fractions of 0.1, 0.15, and 0.75 respectively to simulate the observed tree density.

Vegetation types in ORCHIDEE are grouped into three hydrological tiles with homogeneous soil hydrological properties within a hydrological tile (Boucher et al., 2020). One tile is for bare soil, one for croplands and grasslands, and one for trees. Each hydrological tile represents a distinct soil water column within which PFTs compete for water.

### 2.3.2 Soil and root configuration

The soil representation in the standard configuration of ORCHIDEE is based on a multi-layer physical description of the soil. By default, the soil depth is set at 2 m (Figure 2) and the soil is discretized into 11 layers of increasing thickness following a geometric series with a ratio of two (Campoy et al., 2013; de Rosnay et al., 2002). In the Faidherbia configuration, the soil depth was increased to 7 m (Figure 2), and the soil was discretized into 120 layers following Ducharne et al., (2018) to ensure numerical schemes' stability. A finer resolution was used in the upper soil layers with a geometrical increase of soil layers from surface to 0.15 m (ratio: 1.8) to capture the strong gradient of soil moisture and temperature near the surface. From 0.15 m to 6.5 m, a constant layer thickness of 0.065 m is applied to simplify the model where gradients are less pronounced. Between 6.5 m and 7 m, the geometric progression resumes to ensure numerical stability as strong soil moisture gradients are again modelled as a result of free drainage at the soil bottom.

Soil texture in the standard configuration, defined by the fractions of sandy loam, loam, and clay loam, is homogeneous in the pixel and controls the soil parameters, i.e., field capacity and wilting point, Van Genuchten parameters (Boucher et al., 2020), which are assumed constant through time. In the Faidherbia configuration, soil texture and soil hydrological parameters were taken from Diongue et al., (2022) and Roupsard et al., (2020) as summarized in Table S1.

In the standard configuration, the bottom soil layers allow free drainage which prevents simulating groundwater dynamics. In the Faidherbia configuration, groundwater was simulated by forcing a dynamic water content of soil layers between 4 m and 5 m and imposing water saturation below 5 m, following Campoy et al., (2013). Groundwater forcing was exclusively implemented for the hydrological tile dedicated to tree PFTs.

In the standard model configuration, maximum crop root depth is 0.8 m and maximum tree root depth is 2 m (Figure 2). The root profile, representing the fraction of root mass distributed across each soil layer based on the availability of water, is defined following Eq. (1):

$$
Rf(i) = \begin{cases} 0, & \text{if } i = 1 \\ 0, & \text{if } \sum_{i=2}^{n} \max(0, W_i - W_{p,i}) \leq 0 \\ \frac{\max(0, W_i - W_{p,i})}{\sum_{i=2}^{n} \max(0, W_i - W_{p,i})}, & \text{if } i > 1 \text{ and } \sum_{i=2}^{n} \max(0, W_i - W_{p,i}) > 0 \end{cases} \tag{1}
$$

where i is the index for each soil layer, Rf represents the root profile at position i (unitless) and ranges between 0 and 1, n is the total of soil layers, $W_i$ represents the soil moisture at position i (kg m$^{-2}$) and $W_{p,i}$ represents the wilting point moisture at position i (kg m$^{-2}$).

In the Faidherbia configuration, crop and tree root depths were increased to 2 m and 7 m respectively to match field observations and the root profile was adjusted to be consistent with recent observations of Siegwart et al., (2023). It was assumed that crops use water from soil layers up to 2 m in depth, whereas tree roots take up water from depths below 4 m (Figure 2). Thus from Eq. (1), the adjusted root profile for *Faidherbia albida* is calculated following Eq. (2):

$$
Rf(i) = \begin{cases} 0, & \text{if } i < i_{4m} \\ 0, & \text{if } i \geq i_{4m} \text{ and } \sum_{i=i_{4m}}^{n} \max(0, W_i - W_{p,i}) \leq 0 \\ \frac{\max(0, W_i - W_{p,i})}{\sum_{i=i_{4m}}^{n} \max(0, W_i - W_{p,i})}, & \text{if } i \geq i_{4m} \text{ and } \sum_{i=i_{4m}}^{n} \max(0, W_i - W_{p,i}) > 0 \end{cases} \tag{2}
$$

where i is the index for each soil layer, $i_{4m}$ represents the index of the soil layer at 4 m, Rf represents the root profile at position i (unitless) and ranges between 0 and 1, n is the total of soil layers, $W_i$ represents the soil moisture at position i (kg m$^{-2}$) and $W_{p,i}$ represents the wilting point moisture at position i (kg m$^{-2}$). All soil and root depths, and soil water content parameters used in this study are summarized in Table S1.

### 2.3.3 Phenology and photosynthesis parameters

In the standard configuration, leaf onset for tropical trees is driven by soil moisture constraints on growth (Eamus et al., 2013; Murphy and Lugo, 1986) and is therefore modelled as a function of water stress as calculated over the whole soil column (Botta et al., 2000). The detailed calculation of water stress is provided in the Supplement (Text S1). Leaf onset can be triggered by three conditions: (1) either when a given time has passed since the minimum soil moisture for plant growth was recorded, and (2) the weekly moisture availability is higher than monthly moisture availability, or (3) when the monthly moisture availability exceeds a prescribed critical moisture availability. In the Faidherbia configuration, a time delay was added to these previous water stress conditions based on observations by Roupsard et al., (2022), who found that the first leaves of *Faidherbia albida* appeared on average 30 days after groundwater rise (Figure 2).

In the standard model configuration, the phenology for the crop PFT is based on a combination of growing degree days (Chuine, 2000) and water stress (Botta et al., 2000). In the Faidherbia configuration, a rainfall threshold was added, specifying

230    that leaf onset can only occur if there is a minimum of 10 mm of rainfall either in a single day or over a three-day period (Berg et al., 2010; Marteau et al., 2011; Ndiaye et al., 2024). This constraint prevents leaf emergence from being triggered solely based on water stress conditions that may arise from very minor precipitation events.

In the standard configuration, crops are harvested abruptly just after the senescence stage starts, unlike trees, in which leaf biomass gradually dies during the senescence period. This abrupt crop harvest does not reflect the harvesting practices of

235    farmers in the study region, because the most common practice is to pull or cut the panicle of the millet stalk just below where the grain is formed (Hedayetullah and Zaman, 2022). The stalks can then be harvested from 80 cm above the ground (Kajuna, 2021; Lericollais, 1999), leaving some leaves which regrow at the internodes and thus allowing photosynthetic processes to continue before complete stalk mortality. In the Faidherbia configuration, in order to represent this process, a parameter was defined as a delay between senescence start and harvest adding a senescence stage in the crop life cycle. The newly defined

240    crop senescence stage reproduces senescence and turnover processes used in the standard model for grasslands (Figure 2) where biomass die-off depends on the growing degree days and leaf lifespan consistent with millet photoperiodism (Adole et al., 2019; Sanon et al., 2014). This adjustment results in a slow biomass decay until harvest when all parts of the crops are removed.

### 2.3.4 Carbon assimilation for trees

245    In the standard configuration, ORCHIDEE simulates C3 plant leaf-level photosynthesis using the extended Farquhar et al., (1980) model from Yin and Struik, (2009). This model considers the influence of rubisco activity (Vcmax) and electron transport rate (Jmax) on $CO_2$ assimilation. Most model parameters follow Yin and Struik, (2009) except Vcmax and Jmax, which are constrained by nitrogen use efficiency and acclimate to growth temperature (Kattge and Knorr, 2007; Medlyn et al., 2002). In the standard configuration, Vcmax is calculated from leaf nitrogen content at the top of the canopy and nitrogen use

250    efficiency (NUE) of Vcmax which is prescribed for each PFT. In contrast, Jmax is calculated from the ratio, a function of growth temperature between Jmax and Vcmax (Kattge and Knorr, 2007). In the Faidherbia configuration, site observations of Vcmax and Jmax were used to parameterize NUE and Jmax (section 2.2.3).

### 2.4 Climate input data sets

ORCHIDEE requires climate input data of air temperature (°C), precipitation (mm), relative humidity (%), atmospheric

255    pressure (hPa), wind speed (m s$^{-1}$), shortwave radiation (W m$^{-2}$), and long-wave radiation (W m$^{-2}$). Although ORCHIDEE is run at the half-hourly time step, the data could be at the half-hourly to 6-hourly time-step. If the frequency of the data is less than half-hourly, ORCHIDEE interpolates the climate forcing in between two data points. Three climate data sources were used as inputs in this study:

(1) When no in-situ climate data were available (i.e. before 2018), CRUJRA v2.2.2 produced by the Climatic Research Unit (CRU) (Harris et al., 2020) and Japanese reanalysis (JRA) data (Kobayashi et al., 2015) were used. CRUJRA provides a 6-hourly, 0.5-degree global reconstruction from 1901 to 2020.

(2) In-situ observations of meteorological variables were available from the Faidherbia-flux observatory with half-hourly measurements from 2018 to 2023 (Text S2 and Fig. S2 in the Supplement). In-situ measurements started on 22 February 2018 and thus contain a gap from January 1$^{st}$ to February 21$^{st}$ of 2018. To address this issue, the meteorological data were gapfilled following Vuichard and Papale, (2015). The gap-filling procedure relies on the ERA Interim climate reanalysis. ERA Interim is the latest atmospheric reanalysis product provided by the European Centre for Medium-Range Weather Forecasts (ECMWF) (Dee et al., 2011). It offers data from 1989 to present on a regular spatial grid of 0.7 degrees and a temporal resolution of 3 hours.

(3) To eliminate artifacts that would occur when switching from CRUJRA to in-situ observations, a statistical linear correction was applied to CRUJRA data for the period 1963-2017. This correction aligned the mean values of the common years in CRUJRA (2018-2020) with those observed in the data from 2018-2020, following the approach proposed by Vuichard and Papale, (2015) for ERA Interim. This method corrects biases in CRUJRA data by establishing a linear relationship with an observed dataset for most meteorological variables. The regression coefficients for global radiation and wind speed fields were calculated with an intercept forced to zero to prevent negative radiation values and an excessively flat regression slope for wind speed. An alternative method, based on ratios was used for precipitation data due to timing inaccuracies, i.e., the moment of precipitation may differ between the CRUJRA and the in-situ observations. The ratio between the sum of monthly rainfall in CRUJRA and the sum of monthly rainfall in the observed data was calculated. The de-biased precipitation field was then obtained by multiplying CRUJRA rain data by this ratio.

## 2.5 Simulation protocol

The simulation protocol consists of the following eight runs: (1) spin-up, (2) $CO_2$ transient, (3) climate transient, (4) clear-cut, (5) experiment, (6) calibration, (7) evaluation, and (8) sensitivity runs. Runs (1) to (4) include only the tree PFT, while runs (5) to (8) include both tree and crop PFTs. The details of each run are provided below:

(1) The spin-up run aims at initializing the soil and litter carbon and nitrogen masses and is run until an equilibrium of the system's carbon, nitrogen and water pools is achieved. For this, the spin-up consists of a 500-year semi-analytical spinup with the entire pixel assumed to be covered by tropical deciduous summergreen trees, weather cycling over the 1901 to 1910 time series of meteorological variables (CRUJRA) and atmospheric $CO_2$ concentration fixed at the 1860 level and thus equal to 286.42 ppm.

(2) A first transient run aims at including the effect of rising $CO_2$ on the carbon, nitrogen and water fluxes and the carbon pools. For this, a 40 years transient simulation is run with weather still cycling over the 1901-1910 meteorological forcing and the atmospheric $CO_2$ progressively increasing from 286.45 ppm to the 1901 level of 296.57 ppm.

11

(3) A second transient run aims at matching climate and $CO_2$ historical levels. It consists of 60 years run with 1901-1961 CRUJRA climate forcing and linear increase in $CO_2$ from 296.80 ppm to 317.09 ppm.

(4) A clear-cut run aims at constraining the trees' ages to match the observed average tree age of 55 years in 2017. It
295  consists of a one-year run for 1962 with a forest clear-cut. Living biomass is removed and transferred to the litter pools before a new stand can grow.

(5) A 55-year experimental simulation (1963-2017) aims at getting the ecosystem to the 2018 conditions through simulated growth. It consists of 55 years run with tree and crop cover forced with 1963-2017 CRUJRA climate forcing data and historical atmospheric $CO_2$ concentration increasing from 318.40 ppm to 404.71 ppm.

300 (6) A calibration simulation was run to adjust model parameters. For this, a 3-year simulation for years 2018-2020 was run (section 2.6) with climate forcing from observed in situ climate data (section 2.4). After obtaining the calibrated parameters from step 6, steps 1 to 6 were then repeated with those parameters.

(7) The evaluation simulation aiming at evaluating the robustness of model calibration with previously unseen data relied on a 2021-2023 simulation with observed in situ climate data.

305 (8) Sensitivity runs aim at evaluating the effect of tree density or water (rain and water in the capillary fringe of the groundwater) availability on ecosystem functioning (section 2.8). They consist of 3- or 6-years long simulations using observed in situ climate data and scenarios of tree density and water availability.

## 2.6 Model calibration

First, model allometry was calibrated by adjusting the parameters related to tree allometric properties, such as wood density,
310 form factor for cylinder volume reduction, and height factors (Table S1) until trees dimensions approximately matched observed diameters and height presented in section 2.1.

In a second step, parameters determining the start and end of the growing season in the model phenology, including minimum time since season start, minimum time elapsed, leaf longevity, and length of leaf senescence (Table S1), were adjusted through visual comparison of simulated and observed LAI on three years for crops (2018-2020) and two years for trees (2019-2020).
315 For crops and trees subsequently, starting from model default values, parameters were increased or decreased until dry and wet season dynamics for LAI were within less than 7 days of observed data.

In a third step, crop and tree carbon and energy fluxes were calibrated sequentially focusing on LAI, GPP, latent (LE) and sensible (H) heat. For this, three years for crops (2018-2020) and two years for trees (2019-2020) of observed and simulated data were compared using root mean square error (RMSE). In this third step, parameters were incrementally varied until a
320 local minimum was reached for RMSE. The leaf-to-sapwood area ratio was adjusted for LAI until local minimization of RMSE and an acceptable maximum LAI value was reached (Table S1). For GPP, parameters associated with photosynthesis and carbon allocation, such as light absorption efficiency, electron transport, and Rubisco kinetics, were adjusted until local

minimization of RMSE and an acceptable maximum GPP value was achieved (Table S1). Due to interaction between LAI and GPP variables, calibration of GPP called for a second adjustment loop of the leaf-to-sapwood area ratio. As a result of the large uncertainties in LAI compared to GPP measurements, priority was given to GPP seasonal maximum calibration. For the energy flux (LE and H), evapotranspiration and vegetation structure parameters were fine-tuned to ensure consistency with observed LE and H patterns aiming for minimized RMSE and a realistic maximum of LE and H.

## 2.7 Model evaluation performance

To ensure the obtained calibrated parameters were not too dependent on the specific years and on the variables used for calibration, three years of observations (2021-2023) were used to evaluate the model fitness outside the calibration conditions. Simulations were compared against daily observations of LAI, GPP, LE, H and net radiation as well as annual total GPP with RMSE and $r^2$ as indicators of model fitness. Statistical analysis in the calibration and evaluation were performed using Python v3.9 (Python Software Foundation – available at http://www.python.org).

## 2.8 Sensitivity analysis

Two sensitivity analyses were performed in order to determine:

(1) the sensitivity of ecosystem GPP, above-ground harvested crop biomass and energy fluxes (LE and H) to tree density. For this, four planting densities were applied to the model: 0 trees ha$^{-1}$, 7 trees ha$^{-1}$, 13 trees ha$^{-1}$ (observed density in the plot), and 26 trees ha$^{-1}$. Since ORCHIDEE uses a self-thinning relationship that links stand density to tree diameter, the PFTs proportions rather than the actual densities were adjusted in the pixel to obtain the expected tree densities over the whole pixel. Assuming an average crown area of 116 m² for 13 trees ha$^{-1}$, tree densities of 0, 7, 13, and 26 trees ha$^{-1}$ respectively corresponded to 0 %, 7.5 %, 15 %, and 30 % tree PFT fraction in the pixel (Table S2).

Statistical analyses were performed using the "stats" package (v4.41) within R software (R Core Team, 2024). The suitability of data for parametric tests was assessed by checking for variance homogeneity with the Bartlett test and evaluating residuals for normality using the Shapiro-Wilk test. One-way ANOVAs were applied when these conditions were satisfied. When assumptions for parametric tests were not met, the Kruskal-Wallis test, a non-parametric alternative, was employed. Post-hoc pairwise comparisons for ecosystem GPP and above-ground harvested crop biomass were conducted using Tukey's honestly significant difference test.

(2) the sensitivity of GPP and energy fluxes (LE and H) to year-to-year fluctuations in rainfall and soil water content in the capillary fringe of the groundwater table (SWCC). For this, the average yearly cycle of precipitation and groundwater dynamics were respectively computed to be used as multi-year time series without any interannual variability. These are called the "average" scenarios (see Text S3 and Fig. S3 for details on the calculation in the Supplement). The sensitivity analysis consisted of four climate and SWCC combinations: i) simulation with average rain and average SWCC ($R_{avg}SWCC_{avg}$), ii) simulation with average rain and variable SWCC ($R_{avg}SWCC_{var}$), iii) simulation with variable rain and average SWCC

($R_{var}SWCC_{avg}$) and iv) simulation with variable rain and variable SWCC ($R_{var}SWCC_{var}$). In all simulations, the other climate

355    forcing variables were taken from CRUJRA climate forcing data.

The sensitivity is quantified as the anomaly of all scenarios with respect to $R_{avg}SWCC_{avg}$ considered as the reference scenario. The anomalies in SWCC, GPP, LE and H for Faidherbia trees (scenario $R_{avg}SWCC_{var}$), due to their staggered growth cycle, were analyzed from the beginning of October in year n to the end of June in year n+1. In contrast the anomalies in rainfall, GPP, LE and H for crops (scenario $R_{avg}SWCC_{var}$) were analysed over a three-month period from the beginning of July to the

360    end of September of the same year. Given the variability of both rainfall and SWCC in the scenario $R_{var}SWCC_{var}$, anomalies in GPP, LE, and H at ecosystem level were assessed over annual periods, spanning from July 2019 to September 2021.

## 3 Results

### 3.1 Model evaluation

#### 3.1.1 Phenology (LAI)

365    For trees, the 'reverse phenology' of *Faidherbia albida* with its growing season in the dry season was reproduced by the model with an $r^2$ between daily tree LAI simulation and observation of 0.81 (n=1095) and an RMSE of 0.15. Simulated and observed peaks in LAI were aligned with the dry growing season and the wet dormant season of this tree species (Figure 3e). Over the evaluation period, a maximum measured tree LAI of 0.81 was recorded, while maximum simulated LAI values reached 0.73. However, 2 out of 3 years, the maximum tree LAI was overestimated by the model by 11 % and 13 % in 2020-2021 and 2022-

370    2023 respectively (Figure 3e). The interannual variability of the simulated tree LAI was lower in the simulations than in the observations with a standard deviation of the maximum LAI of 0.002 in simulations compared to 0.09 in observations, and a standard deviation of the maximum LAI day relative to the emergence day is 1 day in simulations and 17 days in observations over the evaluation period (Figure 3e).

Regarding crops, the model simulated a maximum daily LAI of 0.90 compared to the observed maximum daily crop LAI of

375    1.20 with an RMSE of 0.26 over the evaluation period (Figure 3f). With a single parameter set being used irrespective of the crop species, the model goodness-of-fit did not appear to depend on the actual crop sown. The day of maximum LAI was simulated with a delay of +17, -7, -10 days in 2021 to 2023 respectively (Figure 3f). For crops, similar to trees, the model underestimated the interannual variability of LAI over the evaluation period. Specifically, the maximum crop LAI was underestimated by 28 %, 24 %, and 22 % in 2021, 2022, and 2023, respectively (Figure 3f).

380
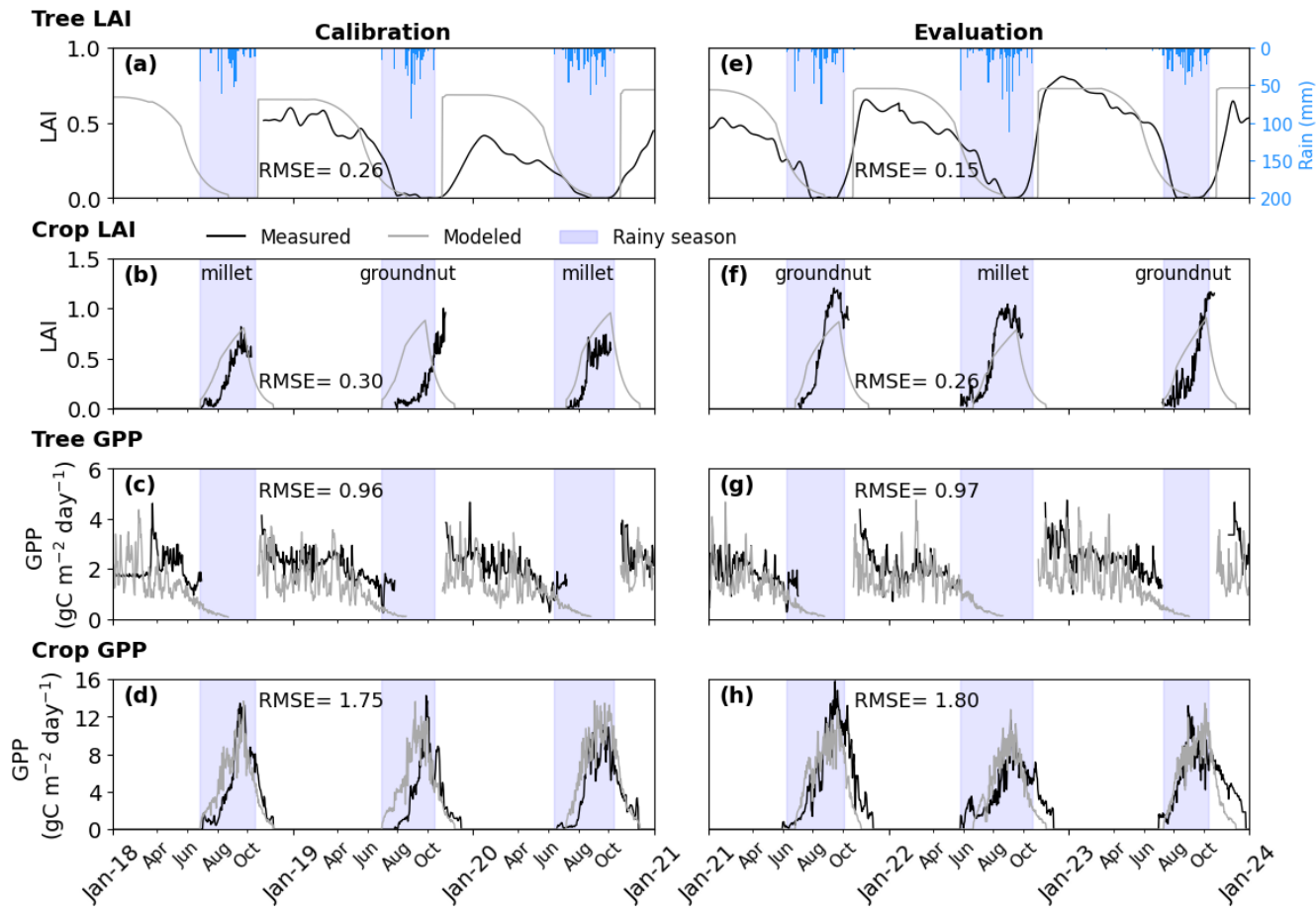


**Figure 3: Measured and modeled time series at the daily time-step for calibration and evaluation periods for (a, c, e, g) tree and (b, d, f, h) crop, showing leaf area index (LAI) and gross primary productivity (GPP), respectively. The crops, millet and groundnut, are cultivated in an annual rotation. Shaded blue areas indicate the rainy season. Annual rainfall from 2018 to 2023 was 454.43 mm,**
385     **513.05 mm, 599.34 mm, 482 mm, 821.62 mm, and 537.83 mm, respectively.**

### 3.1.2 Carbon sequestration (GPP)

The observed daily tree GPP reached a peak value of 4.74 gC m$^{-2}$ day$^{-1}$, closely matched by the model's maximum prediction of 4.75 gC m$^{-2}$ day$^{-1}$ (Figure 3g). During the evaluation period, the r$^2$ between simulation and observation of the daily tree GPP was 0.16 (n=666) and RMSE of 0.97 gC m$^{-2}$ day$^{-1}$. However, the model consistently underestimated the annual GPP of

390     trees, with errors ranging from 2 % to 22 % throughout the evaluation period (Table 1).

For crops, the observed daily GPP peaked at 15.76 gC m$^{-2}$ day$^{-1}$, while the model's maximum prediction was lower, at 13.41 gC m$^{-2}$ day$^{-1}$ (Figure 3h). The RMSE for daily crop GPP was 1.80 gC m$^{-2}$ day$^{-1}$, and the r$^2$ between simulated and observed

15

values was 0.76 in the evaluation (n = 1095; Figure 3d). The model underestimated the peak daily crop GPP in 2021 (Figure 3h). On an annual scale, the crop GPP was underestimated by 9 % to 19 % between 2021 and 2023 (Table 1).

395 For the whole ecosystem, the total annual GPP was underestimated by 18 %, 6 %, and 16 % in 2021, 2022, and 2023, respectively (Table 1). Tree contributions to the total annual ecosystem GPP varied between 32 % and 37 % in observations and between 33 % and 37 % in simulations during the 2021–2023 period.

**Table 1: Annual GPP for simulated and measured tree and crop gross primary productivity at the annual time step.**

| Annual GPP | | Calibration | | | Evaluation | | | |
| --- | --- | --- | --- | --- | --- | --- | --- | --- |
| | | 2018 | 2019 | 2020 | 2021 | 2022 | 2023 | mean ± standard deviation |
| Tree | Observed (tC ha$^{-1}$ yr$^{-1}$) | 5.22 | 5.51 | 5.12 | 4.76 | 4.23 | 5.51 | 5.06 ± 0.49 |
| | Modeled (tC ha$^{-1}$ yr$^{-1}$) | 4.31 | 3.77 | 3.93 | 4.03 | 4.14 | 4.31 | 4.08 ± 0.21 |
| | Relative bias (%) | -17 | -32 | -23 | -15 | -2 | -22 | — |
| Crop | Observed (tC ha$^{-1}$ yr$^{-1}$) | 6.81 | 5.41 | 7.07 | 10.02 | 7.81 | 9.58 | 7.78 ± 1.75 |
| | Modeled (tC ha$^{-1}$ yr$^{-1}$) | 7.26 | 7.47 | 9.49 | 8.11 | 7.12 | 8.35 | 7.97 ± 0.89 |
| | Relative bias (%) | 7 | 38 | 34 | -19 | -9 | -13 | — |
| Ecosystem scale | Observed (tC ha$^{-1}$ yr$^{-1}$) | 12.03 | 10.92 | 12.19 | 14.79 | 12.04 | 15.10 | 12.84 ± 1.69 |
| | Modeled (tC ha$^{-1}$ yr$^{-1}$) | 11.57 | 11.24 | 13.42 | 12.15 | 11.26 | 12.66 | 12.05 ± 0.87 |
| | Relative bias (%) | -4 | 3 | 10 | -18 | -6 | -16 | — |

400 **3.1.3 Energy budget (LE, H and Rn)**

The daily simulated latent heat flux reached a maximum of 11.56 MJ m$^{-2}$ day$^{-1}$ compared to the daily observed maximum of 12.66 MJ m$^{-2}$ day$^{-1}$ in the evaluation (Figure 4d). The model tended to overestimate low daily latent heat flux values by the end of the dry seasons between 2021 and 2023. The evaluation yielded an RMSE of 2.12 MJ m$^{-2}$ day$^{-1}$ and a correlation between simulated and observed daily latent heat flux of 0.49 (n=1095) (Fig. 4d and 4g).

405 The maximum simulated sensible heat flux was 11.42 MJ m$^{-2}$ day$^{-1}$, exceeding the observed maximum of 9.46 MJ m$^{-2}$ day$^{-1}$ between 2021 and 2023 (Figure 4e). The evaluation indicated an r² of 0.67 and an RMSE of 2.40 MJ m$^{-2}$ day$^{-1}$ for daily sensible heat flux (n = 1095). However, the model consistently overestimated both low and high daily sensible heat flux values (Figure 4e and 4h).

For net radiation, the simulated daily maximum was 16.08 MJ m⁻² day⁻¹, higher than the observed daily maximum of 14.42

410 MJ m⁻² day⁻¹ in the evaluation (Figure 4f). Between 2021 and 2023, the model consistently overestimated daily net radiation during the dry season. Over the evaluation period, the RMSE was 2.31 MJ m⁻² day⁻¹, and the model explained 72 % of the variability in observed daily net radiation (Figure 4f and 4i).
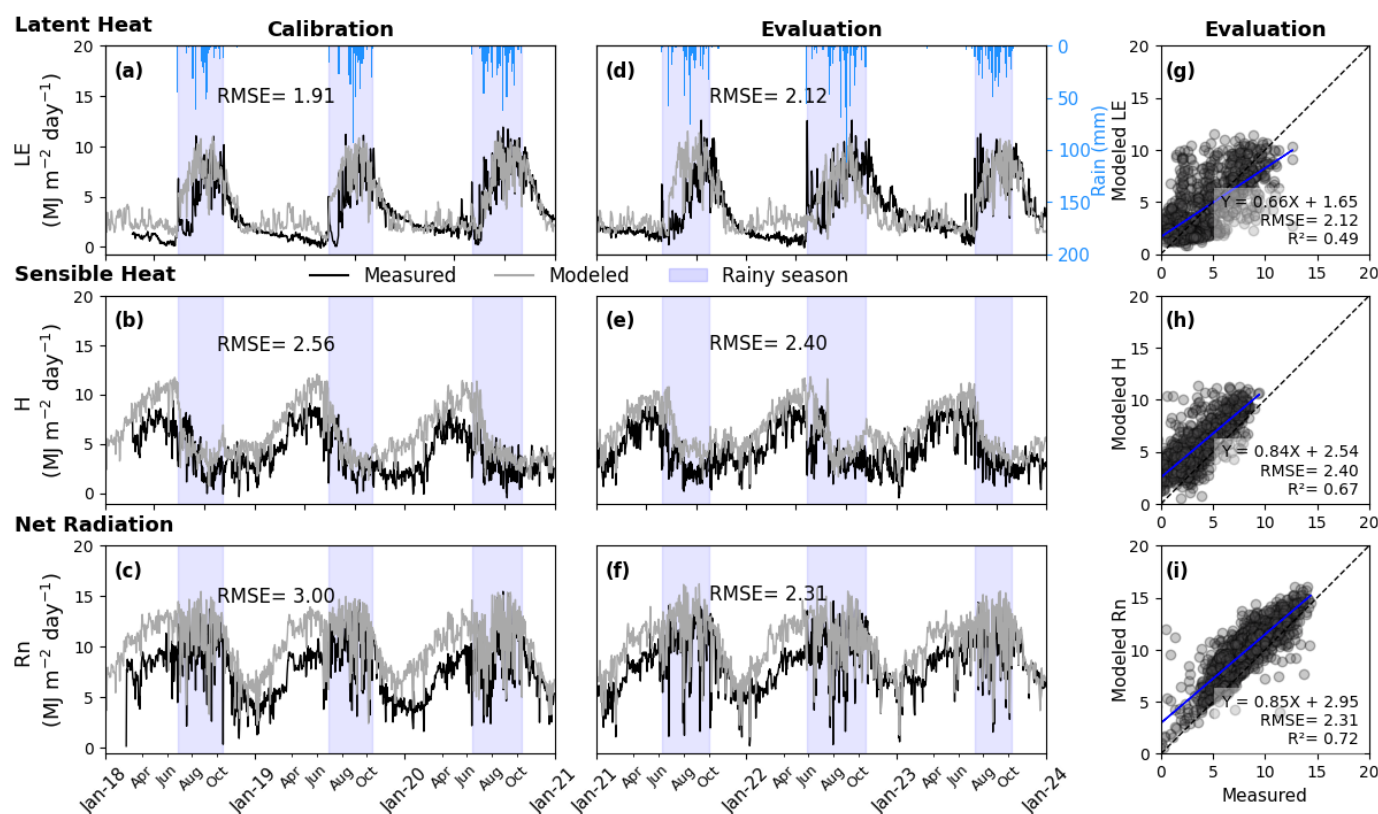


415 **Figure 4: Daily time series (left) and scatter plots (right) comparing modeled and measured (a, d, g) latent heat flux (LE), (b, e, h) sensible heat flux (H), and (c, f, i) net radiation (Rn). The left panels show calibration and evaluation periods, while the right panels focus on evaluation scatter plots. Shaded blue areas indicate the rainy season. Annual rainfall from 2018 to 2023 was 454.43 mm, 513.05 mm, 599.34 mm, 482 mm, 821.62 mm, and 537.83 mm, respectively. The dashed line represents the 1:1 line, while the solid blue line depicts the linear regression line.**

420 **3.2 Ecosystem sensitivity to tree density**

Varying tree density (0, 7, 13, and 26 trees per hectare) significantly influenced annual GPP during the dry season (Kruskal-Wallis, n = 24, p < 0.001; Table 2). Annual GPP increased during the dry season (when Faidherbia trees grow) with tree density, ranging from 0 tC ha⁻¹ yr⁻¹ at 0 trees ha⁻¹ to 8.64 ± 0.84 tC ha⁻¹ yr⁻¹ at 26 trees ha⁻¹ (Table 2). In contrast, during the rainy season, when crops grow and Faidherbia trees are dormant, tree density had no significant effect on annual GPP for

425 densities of 0 to 7 trees ha⁻¹. However, from the densities of 13 to 26 trees ha⁻¹, annual GPP decreased from 7.96 ± 0.89 tC

17

ha$^{-1}$ yr$^{-1}$ to 6.33 ± 0.86 tC ha$^{-1}$ yr$^{-1}$ (Table 2). Across the entire ecosystem, regardless of season, annual GPP was significantly higher at 26 trees ha$^{-1}$ (14.97 ± 1.32 tC ha$^{-1}$ yr$^{-1}$) compared to 0 trees ha$^{-1}$ (9.91 ± 0.64 tC ha$^{-1}$ yr$^{-1}$) (ANOVA, n = 24, p < 0.001; Figure 5a and Table 2).

Above-ground harvested crop biomass decreased with increasing tree density. Biomass was not significantly different between
430   0 and 7 trees ha$^{-1}$ (3.33 ± 0.26 tC ha$^{-1}$ yr$^{-1}$ and 3.1 ± 0.28 tC ha$^{-1}$ yr$^{-1}$, respectively), nor between 7 and 13 trees ha$^{-1}$ (2.77 ± 0.33 tC ha$^{-1}$ yr$^{-1}$). However, biomass at 13 trees ha$^{-1}$ was significantly lower than at 0 trees ha$^{-1}$, and a further significant reduction was observed at 26 trees ha$^{-1}$ (2.08 ± 0.34 tC ha$^{-1}$ yr$^{-1}$) (Figure 5b and Table 2).

During the dry season, tree density significantly affected ecosystem LE (ANOVA, n = 24, p < 0.001), with higher densities resulting in higher LE values, ranging from 0.12 ± 0.07 GJ m$^{-2}$ yr$^{-1}$ at 0 trees ha$^{-1}$ to 0.85 ± 0.12 GJ m$^{-2}$ yr$^{-1}$ at 26 trees ha$^{-1}$
435   (Table 2). In the rainy season, LE did not significantly differ between 0 and 7 trees ha$^{-1}$ (0.72 ± 0.07 and 0.7 ± 0.07 GJ m$^{-2}$ yr$^{-1}$, respectively) but showed a slight reduction at 13 trees ha$^{-1}$ (0.67 ± 0.06 GJ m$^{-2}$ yr$^{-1}$) and a significant decrease at 26 trees ha$^{-1}$ (0.58 ± 0.07 GJ m$^{-2}$ yr$^{-1}$, p < 0.01, Table 2). No significant effect of tree density on ecosystem H was observed during the dry season at densities of 0 to 13 trees ha$^{-1}$, with values ranging from 1.73 ± 0.11 to 1.61 ± 0.1 GJ m$^{-2}$ yr$^{-1}$. However, at 26 trees ha$^{-1}$, H decreased significantly to 1.51 ± 0.12 GJ m$^{-2}$ yr$^{-1}$ (p < 0.01, Table 2). In the rainy season, H did not significantly
440   differ between 0 and 7 trees ha$^{-1}$ (0.33 ± 0.03 and 0.35 ± 0.04 GJ m$^{-2}$ yr$^{-1}$, respectively) but increased slightly at 13 trees ha$^{-1}$ (0.38 ± 0.03 GJ m$^{-2}$ yr$^{-1}$) and significantly at 26 trees ha$^{-1}$ (0.43 ± 0.06 GJ m$^{-2}$ yr$^{-1}$, p < 0.01, Table 2).

**Table 2: Annual statistical summary of gross primary productivity (GPP in tC ha$^{-1}$ yr$^{-1}$), energy fluxes (LE and H in GJ m$^{-2}$ yr$^{-1}$) and crop harvest (tC ha$^{-1}$ yr$^{-1}$) across tree densities (0, 7, 13, and 26 trees); n = 24 and number followed by different letters are**
445   **significantly different.**

| Season | Variable | mean ± standard deviation | | | | Test | p-value |
|--------|----------|----------|----------|----------|----------|------|---------|
| | | 0 trees | 7 trees | 13 trees | 26 trees | | |
| Dry | Tree GPP | 0 ± 0d | 2.16 ± 0.21c | 4.08 ± 0.21b | 8.64 ± 0.84a | Kruskal-Wallis | <0.001 |
| | LE | 0.12 ± 0.07d | 0.33 ± 0.08c | 0.62 ± 0.1b | 0.85 ± 0.12a | ANOVA | <0.001 |
| | H | 1.73 ± 0.11a | 1.74 ± 0.11a | 1.61 ± 0.1ab | 1.51 ± 0.12b | ANOVA | <0.01 |
| Rainy | Crop GPP | 9.91 ± 0.64a | 9.28 ± 0.71a | 7.96 ± 0.89b | 6.33 ± 0.86c | ANOVA | <0.001 |
| | Crop harvest | 3.33 ± 0.26a | 3.1 ± 0.28ab | 2.77 ± 0.33b | 2.08 ± 0.34c | ANOVA | <0.001 |
| | LE | 0.72 ± 0.07a | 0.7 ± 0.07a | 0.67 ± 0.06ab | 0.58 ± 0.07b | ANOVA | <0.01 |
| | H | 0.33 ± 0.03b | 0.35 ± 0.04b | 0.38 ± 0.03ab | 0.43 ± 0.06a | Kruskal-Wallis | <0.01 |
| - | Ecosystem GPP | 9.91 ± 0.64c | 11.44 ± 0.74b | 12.05 ± 0.87b | 14.97 ± 1.32a | ANOVA | <0.001 |
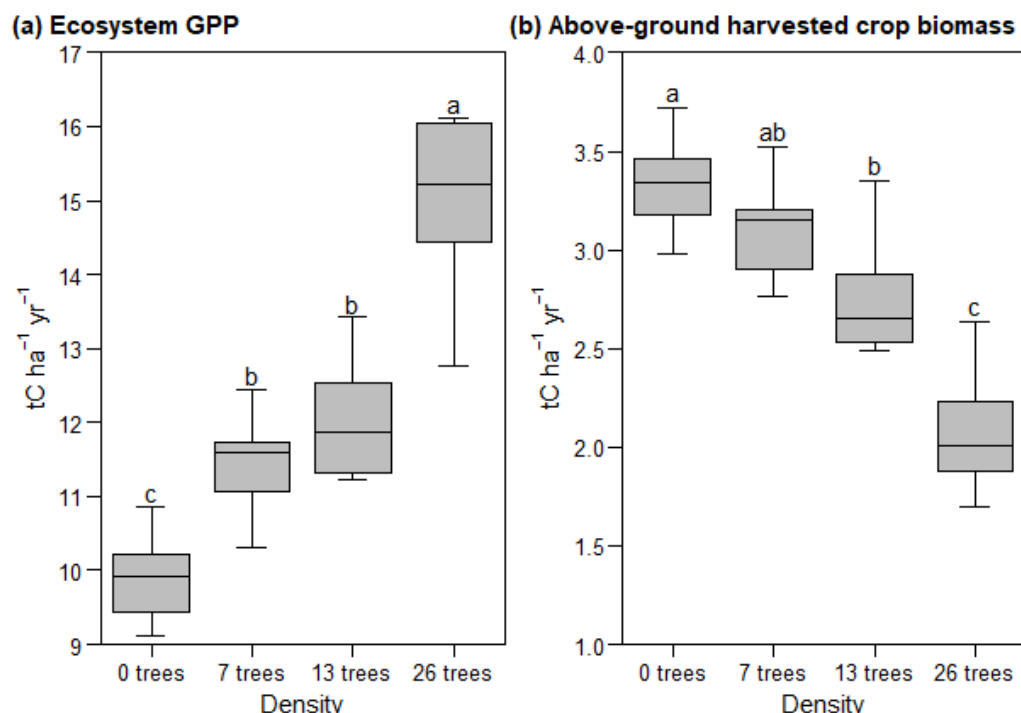
**Figure 5: Effect of the Faidherbia tree density on (a) modeled ecosystem gross primary productivity (GPP) and (b) modeled above-ground harvested crop biomass over six years. The GPP and above-ground harvested crop biomass values represent the annual ecosystem totals for each tree density scenario, averaged over six years. Denotation with different letters indicates significant differences, as revealed by a Tukey (HSD) Post hoc-Test ($\alpha = 0.05$).**

### 3.3 Ecosystem sensitivity to interannual water variability

### 3.3.1 Water variability

Compared to the reference scenario with no variability in the yearly cycle of groundwater availability, $SWCC_{var}$ scenarios mimic: (i) an average deficit of 19 % from October 2019 to June 2020 and (ii) an average excess of 27 % from October 2020 to June 2021 (Figure 6a and S4a). Compared to the reference scenario with no variability in rainfall, the $R_{var}$ scenarios capture distinct rainfall patterns over the study years: (i) an annual rainfall deficit of 63 mm (12 %) in 2019, primarily driven by an early-season deficit of approximately 66 mm in July, (ii) an annual rainfall excess of 53 mm (10 %) in 2020, notably due to an early-season surplus of about 84 mm in July, and (iii) an annual rainfall deficit of 146 mm (28 %) in 2021, characterized by alternating periods of excess, such as 50 mm in July, and deficits, including 134 mm in September (late-season) (Figure 7a and S5a).

### 3.3.2 GPP

As expected, variations in groundwater dynamics only affected tree GPP as the crop roots are too shallow to rely on groundwater (Figure 6). For trees, accounting for groundwater variability resulted in a similar pattern in both years with a decrease in tree GPP compared to the reference at the start of the Faidherbia growing season and an increase in GPP towards

465    the end of the season corresponding to a shift in the growing period of the Faidherbia trees (Figs. 6b and S4b). Since the early-season GPP deficit is larger than the late-season excess, these two response stages combined result in an overall decrease in tree GPP of less than 10 gC m$^{-2}$ yr$^{-1}$, corresponding to approximately 2 % in both 2019–2020 and 2020–2021, during the dry seasons for the R$_{avg}$SWCC$_{var}$ and R$_{var}$SWCC$_{var}$ scenarios (Figs. 6b and 8b).

As expected, rainfall variability primarily influenced crop GPP (Fig. 7a-b), given that tree phenology is shifted to the dry

470    season and tree roots in the model exclusively access groundwater resources. For crops, the GPP response to rainfall variability differed depending on the timing of the anomalies. In 2019, where rainfall was below the reference and early-season deficits were predominant, crop GPP decreased by at least 20 gC m$^{-2}$ yr$^{-1}$ (less than 4 %) under both R$_{var}$SWCC$_{avg}$ and R$_{var}$SWCC$_{var}$ scenarios (Figs. 7b and 8d). Conversely, in 2020, the rainfall surplus, particularly in early-season, led to an increase in crop GPP, with gains of approximately 65 gC m$^{-2}$ yr$^{-1}$ (11 %) under the same scenarios. Despite a severe late-season rainfall deficit

475    in 2021, crop GPP did not show a corresponding decline. Instead, early-season rainfall excess appeared to offset the deficit, resulting in a crop GPP increase of about 86 gC m$^{-2}$ yr$^{-1}$ (14 %) for both scenarios (Figs. 7c and 8c).

At the ecosystem level, in the R$_{var}$SWCC$_{var}$ scenario, where both rainfall and soil water content in the capillary fringe of the groundwater table varied (Fig. 8a-d), simulations indicated a decrease in ecosystem GPP of approximately 78 gC m$^{-2}$ yr$^{-1}$ (about 8 %) in 2019. In contrast, during 2020 and 2021, ecosystem GPP increased by 10 % to 14 %, corresponding to

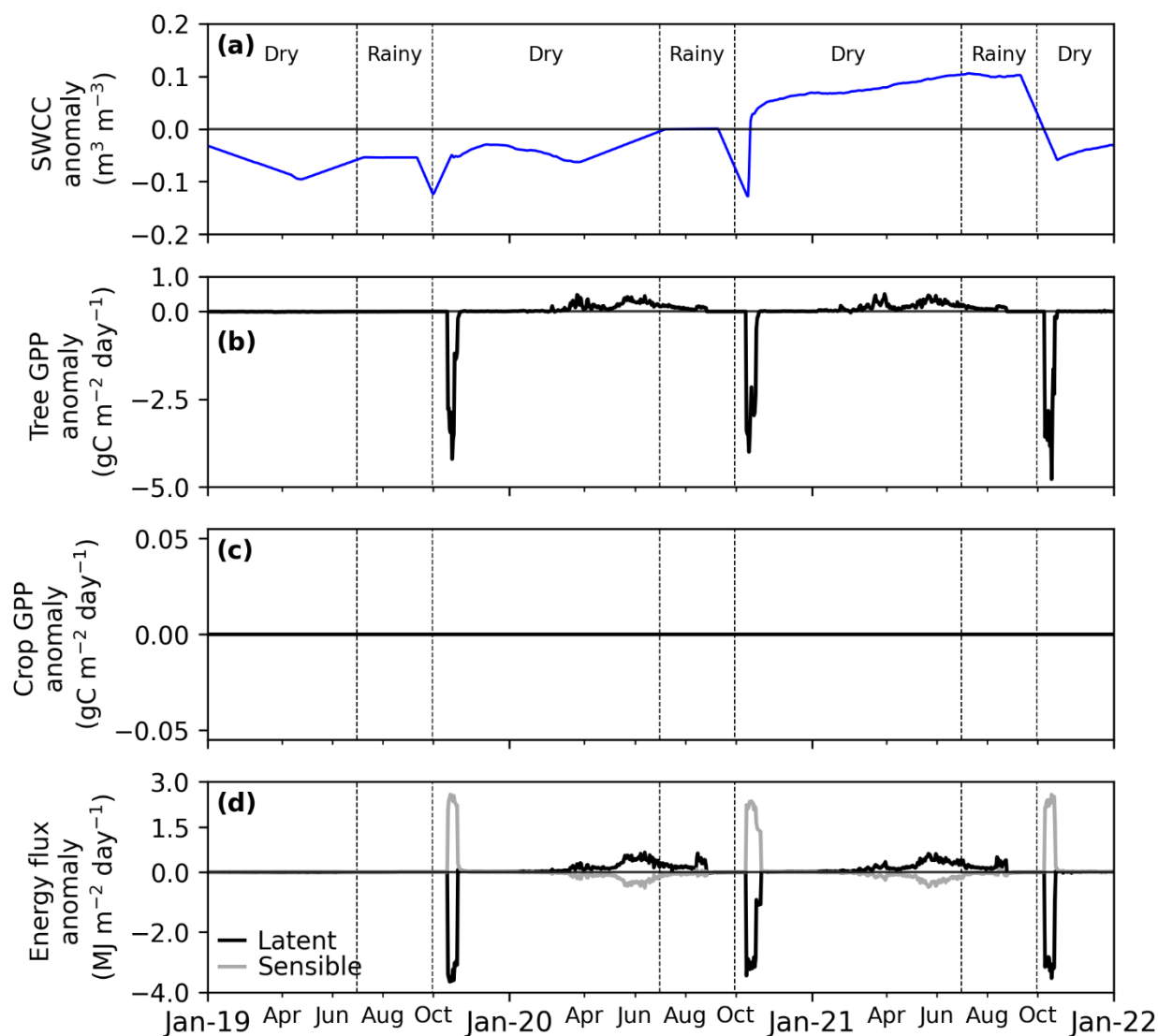480    approximately 118 gC m$^{-2}$ yr$^{-1}$.

**Figure 6: Sensitivity study of the effect of daily anomalies in soil water content in the capillary fringe of the groundwater table (SWCC) with rainfall unmodified: (a) soil water content in the capillary fringe of the groundwater table (SWCC), (b) tree gross primary productivity (GPP), (c) crop GPP anomaly, (d) latent and sensible flux anomaly. RavgSWCCvar is a simulation with average rain and variable SWCC, thus affecting the tree and the ecosystem, but not the crop. The sensitivity is quantified as the anomaly of the RavgSWCCvar scenario with respect to RavgSWCCavg (simulation with average rain and average SWCC), considered as the reference scenario.**
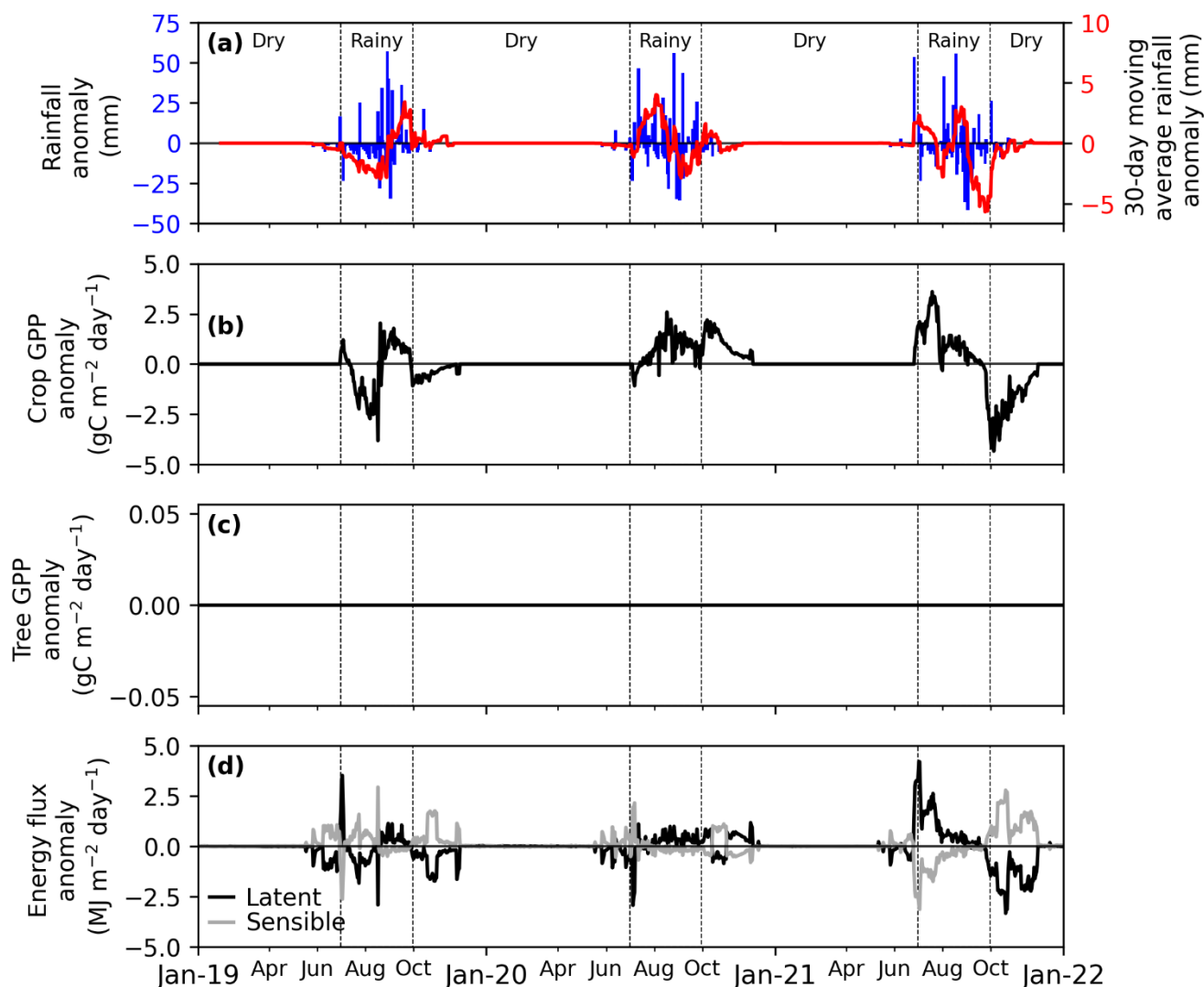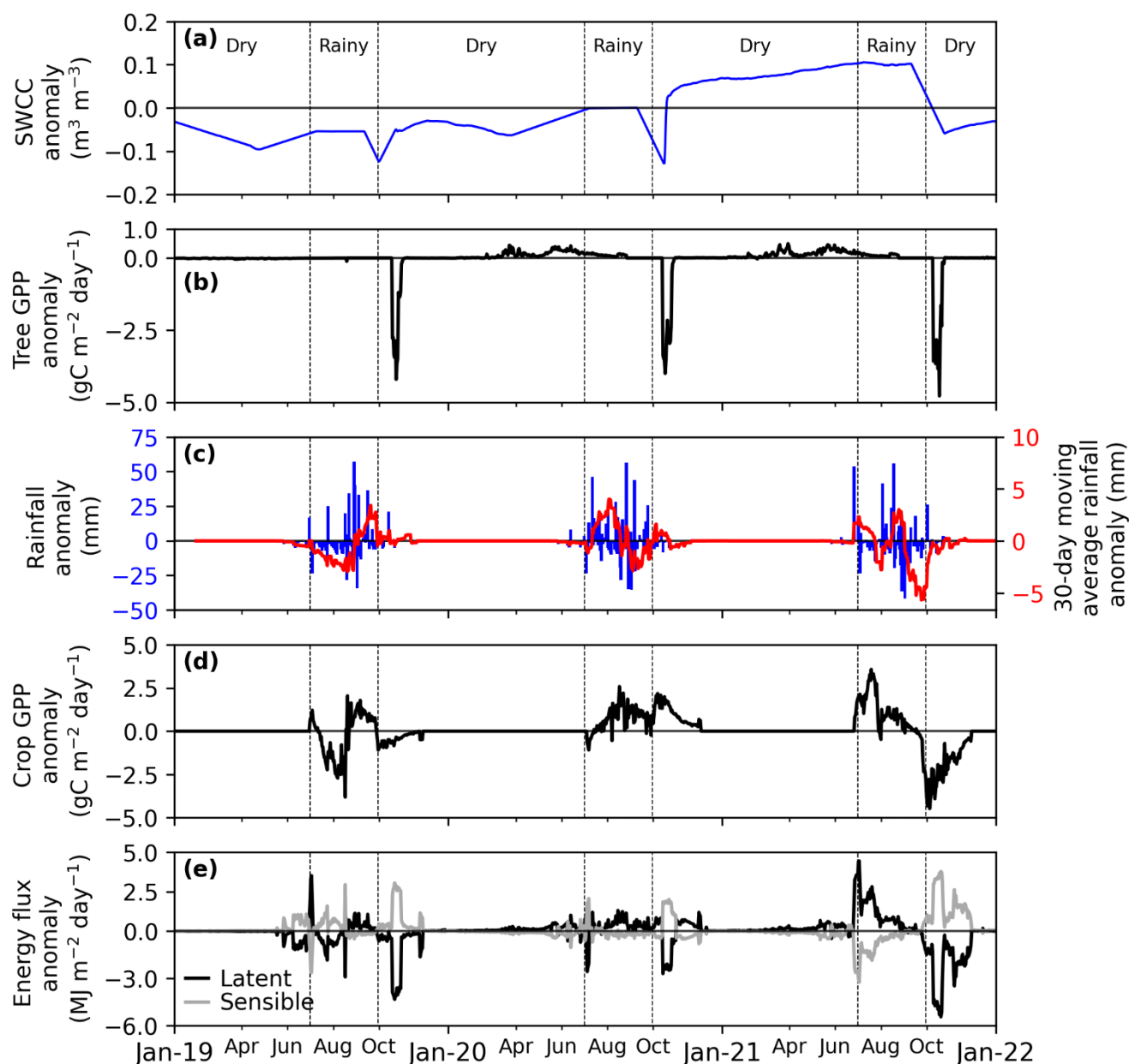
485

**Figure 7: Sensitivity study of the effect of daily anomalies in rainfall (SWCC unmodified) (a) rainfall anomalies: daily (in blue line) and 30-day moving average (in red line), (b) crop gross primary productivity (GPP) anomaly, (c) tree GPP anomaly, (d) latent and sensible flux anomalies. RvarSWCCavg is a simulation with variable rain and average SWCC, thus affecting the crop and the ecosystem, but not the tree. The sensitivity is quantified as the anomaly of the RvarSWCCavg scenario with respect to RavgSWCCavg (simulation with average rain and average SWCC), considered as the reference scenario.**

**Figure 8: Sensitivity study of daily anomalies in rainfall and in SWCC (a) soil water content in the capillary fringe of the groundwater table (SWCC) anomaly, (b) tree gross primary productivity (GPP) anomaly, (c) rainfall anomaly: daily (in blue line) and 30-day moving average (in red line), (d) crop GPP anomaly, (e) latent and sensible flux. RvarSWCCvar is a simulation with variable rain and variable SWC, where crop, tree, and ecosystem are affected. The sensitivity is quantified as the anomaly of the RvarSWCCvar scenario with respect to RavgSWCCavg (simulation with average rain and average SWCC), considered as the reference scenario.**

### 3.3.3 Energy fluxes (LE and H)

During the dry seasons, energy flux (LE and H) anomalies in the $R_{avg}SWCC_{var}$ scenario were strongly correlated with tree GPP anomalies (Fig. 6b-d). LE decreased by 8 MJ m$^{-2}$ yr$^{-1}$ (<1 %) during 2019–2020 and by 11 MJ m$^{-2}$ yr$^{-1}$ (<1 %) during the 2020–2021 dry season. In contrast, H increased from 5 MJ m$^{-2}$ yr$^{-1}$ to 11 MJ m$^{-2}$ yr$^{-1}$ over the same periods (Figs. 6d and S4d).

In the $R_{var}SWCC_{avg}$ scenario, where only rainfall varied annually, energy flux anomalies were driven by crop GPP anomalies (Fig. 7b-d). LE declined by approximately 2 MJ m$^{-2}$ yr$^{-1}$ (<1 %) in 2019 but increased from 14 MJ m$^{-2}$ yr$^{-1}$ (<3 %) in 2020 to 68 MJ m$^{-2}$ yr$^{-1}$ (10 %) in 2021. During the 2019 rainy season, H increased by approximately 9 MJ m$^{-2}$ yr$^{-1}$ (<3 %), whereas it declined by 2 MJ m$^{-2}$ yr$^{-1}$ (<1 %) in 2020 and by 48 MJ m$^{-2}$ yr$^{-1}$ (11 %) in 2021 (Figs. 7d and S5d).

In the $R_{var}SWCC_{var}$ scenario, energy flux anomalies were influenced by anomalies in tree GPP, crop GPP, and rainfall (Figure 8). Consistent with ecosystem GPP anomalies, LE decreased by approximately 54 MJ m$^{-2}$ yr$^{-1}$ (5 %) in 2019 but increased from 60 MJ m$^{-2}$ yr$^{-1}$ (4 %) in 2020 to 116 MJ m$^{-2}$ yr$^{-1}$ (11 %) in 2021. In 2019, H increased by 41 MJ m$^{-2}$ yr$^{-1}$ (6 %), while it declined by 35 MJ m$^{-2}$ yr$^{-1}$ (<3 %) in 2020 and by 81 MJ m$^{-2}$ yr$^{-1}$ (5 %) in 2021 (Figs. 8e and S6e).

## 4 Discussion

### 4.1 Criteria for the evaluation of a phreatophyte configuration of ORCHIDEE

A configuration of ORCHIDEE r7949 model was developed accounting for phreatophyte behaviour of *Faidherbia albida* trees in Sahelian agroforestry systems. Model developments were evaluated through comparison of simulated variables to observations, which is a measure of the goodness-of-fit, or accuracy, of the model, an approach common for model development and evaluation (Collins et al., 2011; Li et al., 2016; Vuichard et al., 2019). However, model developments should be evaluated, not only in the light of their effect on model's accuracy i.e. ability to reproduce observed data, but also on realism, i.e. similarity with real system and generality i.e. transferability to other cases or systems (Levins, 1966).

In this study, the model's goodness-of-fit was evaluated by comparing simulated LAI, carbon, and energy fluxes to on-site measurements. This choice was dictated by the variables of interest for our simulation experiments. The model simulates tree LAI values that correspond to measured LAI, although it fails to capture the observed interannual variations (Figure 3a and 3e). This limitation can be attributed to the simplistic nature of tree phenology models in ORCHIDEE (MacBean et al., 2015). For crops, simulated LAI values were close to those obtained using the process-based biogeochemical model LandscapeDNDC, which was calibrated with Faidherbia-Flux data from 2018 to 2019 (Rahimi et al., 2021). Although less pronounced than for trees, the model also struggled to capture the interannual variability of crop LAI (Figure 3b and 3f). This limitation stems from both the simplified crop phenology model in ORCHIDEE and the decision to disregard crop species rotation at the site, opting instead to represent crops with a single PFT.

Restricting the evaluation to only the variables targeted in the experiment risks overlooking potential biases in other
530   interconnected processes within ORCHIDEE. Given the model's tight coupling between phenology, energy balance, soil
moisture dynamics, and vegetation carbon dynamics (biomass allocation and turnover), such biases could propagate and
indirectly affect key outcomes. To address this, we assessed the consistency of unmodified processes by visually inspecting
energy fluxes (latent and sensible heat), soil moisture dynamics, and vegetation carbon allocation (GPP, net ecosystem
exchange). This step ensured that unintended feedback did not compromise result reliability.

535   Even though it is not quantified here, we estimate that model realism was improved in this study. This claim is supported by
the addition of processes consistent with observations in the developed configuration. In the standard model configuration,
tree phenology relies solely on rainfall and is synchronized with the rainy season. However, incorporating a dynamic water
table forcing and its influence on phenology increased the similarity between simulations and our current understanding of
ecosystem processes (Roupsard et al., 1999; Sarr et al., 2023). An avenue to further enhance model realism could be to alleviate
540   the full phreatophyte assumption employed here. Although *Faidherbia albida* primarily relies on groundwater for growth, it
has also been observed to use water from superficial soil layers, though the proportion remains unknown. This dual water use
could help explain part of the interannual variation in tree LAI, particularly the high values observed during the dry season of
2023 following the high rainfall in 2022 (Figure 3e). Such hypothesis was not implemented here as we assumed according to
isotope observations (Roupsard et al., 1999) that most transpired water originated from the groundwater table and our focus
545   was on the configuration of a growing season synchronized on groundwater dynamics.

The model's generality is estimated to have decreased in the developed configuration due to site-specific adjustments, despite
the inherent generic nature of ORCHIDEE's structure, equations, and parameters. A qualitative understanding of this loss in
generality can be gained by considering two key aspects of the model. First, the implementation of exogenous forcing in
groundwater dynamics using observed soil water content data limits the applicability of the model configuration to sites or
550   regions where such data are unavailable. Second, the calibration of phenology parameters, which significantly impact growth
variables, is based on data from only one site over three years. This makes it unlikely that the model configuration would be
suitable for sites or years with different climate or soil conditions. The decrease in the model's generality warrants caution in
extrapolating the results of simulation experiments, particularly when considering extreme events like prolonged dry spells,
which are particularly relevant in the Sahelian context. Under such climatic conditions, the model underestimates the
555   ecosystem's sensitivity to critical fluctuations in water availability, in contrast to the observed large impacts on ecosystem
dynamics (Reichstein et al., 2013). The limitation in the model's generality is not specific to our configuration but applies to
all site calibration efforts. This is also true for vegetation parameters, which are typically fixed for each plant functional type.
For example, for the plant functional type "C4 crop," one single parameter set was used for all years in this study, despite
records showing that farmers alternated millet and groundnut every other year. Indeed, millet is sown dry approximately one
560   month before the rainy season begins and germinates with the first rains (Sow et al., 2024), whereas groundnuts require

sufficiently moist soil to ensure good germination (Ntare et al., 2008). As a result, the model is unable to account for the physiological and cultivation differences between these two crops. Avenues to increase the configuration's generality include implementing a fully integrated and dynamic groundwater table that accounts for subsuperficial water runoff. Additionally, species-level parameterization or even dynamic parameters based on the growing environment could further enhance the

565 model's flexibility.

The evaluation criteria in this study highlights the trade-off between accuracy and generality as global models have high generality to represent world ecosystems with a single formalization whereas local studies fine-tune the model for a specific case, losing in generality but reaching higher accuracy. Such trade-off is a common feature of large-scale models. Mahnken et al., (2022) explored this balance in European forest models, leveraging Levins' framework (Levins, 1966) to categorize model

570 performance along accuracy, realism, and generality. As in our case study, their comprehensive evaluation of 13 models revealed that improving one dimension often compromises another, underscoring the difficulty of achieving optimal performance across all three. In contrast, a reciprocity between increases in accuracy and realism is found with more processes being associated with better goodness-of-fit. Despite the difficulty of finding a best trade-off, it is important to highlight that this study serves as a first effort to understand and model phreatophyte ecosystems with inverted phenology in an LSM.

575 **4.2 Increased tree density increases carbon sequestration and latent heat flux**

ORCHIDEE's Faidherbia configuration was used to assess the impact of *Faidherbia albida* density scenarios on carbon and energy fluxes. Our study revealed a positive relationship between tree density and ecosystem GPP (Fig .5a). This relationship was a consequence of increasing tree canopy cover and LAI with trees sequestering more carbon per planted area than crops.

Energy flux analysis showed seasonal variations, with both latent heat and sensible heat responding to tree density, consistent

580 with the simulated changes in tree GPP (Table 2). Higher tree densities lead to increased latent heat during the dry season, likely due to higher transpiration rates of trees (Wang et al., 2020) that overcame the reduction in latent heat in the rainy crop-growing season. This is consistent with the result of Sarr et al., (2023), showing a linear dependency between tree transpiration assessed by sapflow and LAI. The inverse relationship between sensible heat and tree density in the dry season suggested that more trees provide shade, reducing soil heat flux, thereby decreasing the Bowen ratio.

585 ORCHIDEE did not simulate grain yield, a critical indicator for farmers; however, the results showed that increasing tree density reduced the above-ground harvested crop biomass (Figure 5b). In the model, this reduction results from the decrease in crop area, when tree density, hence tree area, increases with crop biomass and carbon stocks being reported per unit area of the entire pixel. The simulated decline in crop biomass therefore reflects the competition for space. The trade-off between maintaining an optimal density of *Faidherbia albida* in agroforestry systems and achieving adequate above-ground harvested

590 crop biomass and carbon stocks suggested an ideal range of 7 to 13 trees per hectare, where the difference remains not significant (Figure 5). This range was consistent with traditional recommendations from the local Sereer community, which

historically maintained approximately 7 trees per field (around 1 ha) to secure sufficient yields for a family's food needs (R. Diatte, pers. Comm.; Lericollais, 1972; Pélissier, 1966).

While many studies have highlighted the benefits of *Faidherbia albida* for both crops and the ecosystem (Diongue et al., 2023;
595 Gning et al., 2023; Siegwart et al., 2022; Sileshi, 2016), recent observations suggest highly complex tree-crop interactions (Clermont-Dauphin et al., 2023). Investigation through model studies requires additional processes to be implemented in the model: (1) even though the *Faidherbia albida*'s root architecture, is partially implemented with a representation of a dense root network below the crop roots, the current model omits the shallow roots reported below the surface (Siegwart et al., 2023), and (2) the observed concentration of water and nutrients in the soil under the canopy of *Faidherbia albida* trees (Siegwart et
600 al., 2022; Sileshi, 2016) creating a fertility 'island effect' that can be linked to aridity and plant traits (Eldridge et al., 2024). The improvement of soil organic matter resulting from higher surface water availability and nutrient accumulation could explain the 'island effect' in the close vicinity of the trees and the progressive reduction in millet yields with increasing distance from the tree (Diene et al., 2024; Roupsard et al., 2020).

Additionally, the feedback between tree groundwater consumption and groundwater recharge is currently omitted, hindering
605 the possibility to draw conclusions on tree survival at high densities, especially in the context of the alternance of long drier and wetter periods in the Sahel. Considering these processes of water and nutrient redistribution would enable accounting for competition both among trees and between trees and crops for water and nutrients, thereby helping to determine an optimal tree density that maximizes carbon sequestration and surface cooling through latent heat flux while sustaining crop production.

**4.3 Divergent GPP and energy fluxes responses of trees and crops to water availability**

610 The similarity in the simulated response of tree GPP in both years with a water deficit at the start of the season but either positive or negative soil water content in the capillary fringe of the groundwater table anomaly during the growing season shows that GPP responds to the timing of the groundwater dynamics rather than total water availability during the growing season. This result appears counterintuitive, as interannual fluctuations in groundwater are typically expected to strongly influence GPP (Madani et al., 2020; Palmer et al., 2023). However, this counterintuitive behaviour is consistent with the model
615 implementation of forced saturated groundwater soil levels that prevents any water limitation. A future research avenue could be to make tree root water uptake in the model implementation more sensitive to water deficits.

The response of crop GPP to interannual rainfall variability underscored the critical importance of the timing and distribution of rainfall anomalies during the growing season. Unlike tree GPP, which remains unaffected due to its modeled reliance on groundwater access, crop GPP is directly influenced by rainfall patterns, reflecting the shallow rooting systems and limited
620 access to deeper water reserves. Crop GPP was highly sensitive to early-season rainfall variability, with deficits, such as in 2019, exposing crops to water shortages during critical growth stages, while surpluses, as in 2020, highlight the benefits of sufficient water availability during early development (Camberlin and Diop, 2003; Zhang et al., 2018). Despite a severe late-

season rainfall deficit in 2021, crop GPP reached a similar level as in 2020, highlighting the interplay between early-season rainfall surpluses and late-season rainfall deficits (Figs. 7 and 8). This suggests that early-season water availability can buffer
625 the effects of subsequent deficits, supporting crop growth and productivity during periods of water stress (Faye et al., 2018; Tovignan et al., 2016).

Given the link between GPP and energy fluxes, as expected, the simulated dry-season energy fluxes remained insensitive to interannual variations in soil water content in the capillary fringe of the groundwater table (Figure 6). Conversely, rainfall variability directly affected energy fluxes, with wet season anomalies driven by interactions between rainfall and crop GPP
630 (Figure 7). Notably, when both rainfall and soil water content in the capillary fringe of the groundwater table were variable, the combined effects revealed amplified energy flux anomalies (Figure 8). Since vegetation modulates energy flux responses (Cicuéndez et al., 2023; Williams and Torn, 2015), efforts must be made to improve the representation of soil-water-vegetation interactions in the model. Indeed, the simulated insensitivity of tree productivity to soil water content variability in this study could limit the model's ability to accurately capture energy flux dynamics and the impacts of interannual hydrological
635 variations in semi-arid ecosystems.

## 5 Conclusion

For this study, a configuration of the ORCHIDEE model was developed to account for the dependence on groundwater of a semi-arid agroforestry system dominated by the reverse phenology and phreatophyte tree *Faidherbia albida*. This new ORCHIDEE configuration was used to study the effect of varying tree density and water availability dynamics (rainfall and
640 soil water content in the capillary fringe of the groundwater table) on carbon and energy fluxes. The ORCHIDEE model demonstrated its capacity to simulate seasonal dynamics of LAI and the annual budget of GPP. Interestingly, the reverse phenology tree (growing during the dry season) was found to contribute significantly to the annual GPP, with around 32 % to 50 % occurring during the dry season. The results of the simulation experiment with varying tree density underscored the critical role of tree density in managing semi-arid ecosystems. Additionally, the analysis of ecosystem sensitivity to interannual
645 water variability underscored the critical importance of rainfall timing and distribution during the wet season for crop productivity. The study also highlighted the need to enhance the responsiveness of tree root water uptake to water variability in the model. Such an adjustment may contribute to a more accurate representation of the impact of soil water content on Faidherbia carbon fluxes and their subsequent influence on energy flux partitioning.

This finding highlights the importance of incorporating the effects of deep-rooted phreatophytic tree species like *Faidherbia*
650 *albida* in LSMs to accurately represent carbon and energy fluxes in semi-arid regions. Overall, this study emphasizes the importance of accurately representing photosynthetic characteristics, vegetation maps, groundwater dynamics and belowground processes in LSMs to improve simulations in semi-arid ecosystems. Numerical models can inform sustainable land management practices and contribute to the broader understanding of semi-arid ecosystems. Several experimental,

monitoring and simulation studies on the Faidherbia-Flux site are currently in progress, and are expected to provide a better

655  understanding of the ecosystem and ecophysiology of *Faidherbia albida*, which could help to further develop the version of ORCHIDEE presented in this study.

## 6 Code and data availability

The ORCHIDEE model (r7949) used in this study is open-source and licensed under the CeCILL (CEA CNRS INRIA Logiciel Libre) license. The model code is archived on Zenodo (https://zenodo.org/records/15313734) (Gaglo et al., 2025b), and

660  installation and usage instructions are provided at https://forge.ipsl.jussieu.fr/orchidee/wiki/Documentation/UserGuide. All climate input data, model outputs, in-situ observations, and analysis scripts used in this study are publicly available on Zenodo at https://zenodo.org/records/15383628 (Gaglo et al., 2025a).

## 7 Author contributions

EKG, EC, AV, OR and SL conceptualized and designed the study. OR, CJ, SS, NV and FD provided all necessary data. EKG,

665  EC and AV developed the ORCHIDEE Faidherbia configuration code, and EKG performed the simulations and the data analysis. EKG prepared the paper with contributions from all co-authors.

## 8 Competing interests

The authors declare that they have no conflict of interest.

## 9 Acknowledgments

670  We thank the students and technicians running the "Faidherbia-Flux" platform (https://lped.info/wikiObsSN/?Faidherbia-Flux) and especially Clémence Chenu, Ablaye Diouf, Ibou Diouf, and Robert Diatte. The "Faidherbia-Flux" research infrastructure and platform are funded by CIRAD, IRD, UMR Eco&Sols, LMI IESOL, ISRA, CERAAS. We gratefully acknowledge the use of the Obelix computing cluster from IPSL, France, which provided access to ORCHIDEE and the essential computing infrastructure that enabled the research presented in this paper. Additionally, the authors thank Philippe Peylin, Catherine Ottle,

675  Agnès Ducharne and Josefine Ghattas for sharing their knowledge of the model.

## 10 Financial supports

This work was publicly funded by the DM-TropAFS project through ANR (the French National Research Agency) under the "Investissements d'avenir" programme with the reference ANR-10-LABX-001-01 Labex Agro and coordinated by Agropolis

## References

685 Adole, T., Dash, J., Rodriguez-Galiano, V., and Atkinson, P. M.: Photoperiod controls vegetation phenology across Africa, Commun. Biol., 2, 1–13, https://doi.org/10.1038/s42003-019-0636-7, 2019.

Antunes, C., Díaz Barradas, M. C., Zunzunegui, M., Vieira, S., Pereira, Â., Anjos, A., Correia, O., Pereira, M. J., and Máguas, C.: Contrasting plant water-use responses to groundwater depth in coastal dune ecosystems, Funct. Ecol., 32, 1931–1943, https://doi.org/10.1111/1365-2435.13110, 2018.

690 Barnes, R. and Fagg, C.: Faidherbia albida: monograph and annotated bibliography, Oxford Forestry Institute, University of Oxford, 2003.

Bastos, A., Naipal, V., Ahlström, A., MacBean, N., Smith, W. K., and Poulter, B.: Semiarid ecosystems, in: Balancing Greenhouse Gas Budgets, Elsevier, 311–335, https://doi.org/10.1016/B978-0-12-814952-2.00012-5, 2022.

Berg, A., Sultan, B., and de Noblet-Ducoudré, N.: Including tropical croplands in a terrestrial biosphere model: application to
695 West Africa, Clim. Change, 104, 755–782, https://doi.org/10.1007/s10584-010-9874-x, 2010.

Botta, A., Viovy, N., Ciais, P., Friedlingstein, P., and Monfray, P.: A global prognostic scheme of leaf onset using satellite data, Glob. Change Biol., 6, 709–725, https://doi.org/10.1046/j.1365-2486.2000.00362.x, 2000.

Boucher, O., Servonnat, J., Albright, A. L., Aumont, O., Balkanski, Y., Bastrikov, V., Bekki, S., Bonnet, R., Bony, S., Bopp, L., Braconnot, P., Brockmann, P., Cadule, P., Caubel, A., Cheruy, F., Codron, F., Cozic, A., Cugnet, D., D'Andrea, F., Davini,
700 P., de Lavergne, C., Denvil, S., Deshayes, J., Devilliers, M., Ducharne, A., Dufresne, J.-L., Dupont, E., Éthé, C., Fairhead, L., Falletti, L., Flavoni, S., Foujols, M.-A., Gardoll, S., Gastineau, G., Ghattas, J., Grandpeix, J.-Y., Guenet, B., Guez, E., Lionel, Guilyardi, E., Guimberteau, M., Hauglustaine, D., Hourdin, F., Idelkadi, A., Joussaume, S., Kageyama, M., Khodri, M., Krinner, G., Lebas, N., Levavasseur, G., Lévy, C., Li, L., Lott, F., Lurton, T., Luyssaert, S., Madec, G., Madeleine, J.-B., Maignan, F., Marchand, M., Marti, O., Mellul, L., Meurdesoif, Y., Mignot, J., Musat, I., Ottlé, C., Peylin, P., Planton, Y.,
705 Polcher, J., Rio, C., Rochetin, N., Rousset, C., Sepulchre, P., Sima, A., Swingedouw, D., Thiéblemont, R., Traore, A. K., Vancoppenolle, M., Vial, J., Vialard, J., Viovy, N., and Vuichard, N.: Presentation and Evaluation of the IPSL-CM6A-LR Climate Model, J. Adv. Model. Earth Syst., 12, e2019MS002010, https://doi.org/10.1029/2019MS002010, 2020.

Camberlin, P. and Diop, M.: Application of daily rainfall principal component analysis to the assessment of the rainy season characteristics in Senegal, Clim. Res., 23, 159–169, https://doi.org/10.3354/cr023159, 2003.

710 Campoy, A., Ducharne, A., Cheruy, F., Hourdin, F., Polcher, J., and Dupont, J. C.: Response of land surface fluxes and precipitation to different soil bottom hydrological conditions in a general circulation model, J. Geophys. Res.-Atmospheres, 118, 10725–10739, https://doi.org/10.1002/jgrd.50627, 2013.

Charreau, C. and Fauck, R.: Mise au point sur l'utilisation agricole des sols de la région de Séfa, Agron. Trop. Sér. 2 Agron. Générale Etudes Tech., 1970.

715 Chuine, I.: A Unified Model for Budburst of Trees, J. Theor. Biol., 207, 337–347, https://doi.org/10.1006/jtbi.2000.2178, 2000.

Cicuéndez, V., Litago, J., Sánchez-Girón, V., Román-Cascón, C., Recuero, L., Saénz, C., Yagüe, C., and Palacios-Orueta, A.: Dynamic relationships between gross primary production and energy partitioning in three different ecosystems based on eddy covariance time series analysis, Front. For. Glob. Change, 6, https://doi.org/10.3389/ffgc.2023.1017365, 2023.

720 Clermont-Dauphin, C., N'dienor, M., Leroux, L., S Ba, H., Bongers, F., Jourdan, C., Roupsard, O., C. Do, F., Cournac, L., and Seghieri, J.: Faidherbia albida trees form a natural buffer against millet water stress in agroforestry parklands in Senegal, BASE, https://doi.org/10.25518/1780-4507.20477, 2023.

Collins, W. J., Bellouin, N., Doutriaux-Boucher, M., Gedney, N., Halloran, P., Hinton, T., Hughes, J., Jones, C. D., Joshi, M., Liddicoat, S., Martin, G., O'Connor, F., Rae, J., Senior, C., Sitch, S., Totterdell, I., Wiltshire, A., and Woodward, S.:
725 Development and evaluation of an Earth-System model – HadGEM2, Geosci. Model Dev., 4, 1051–1075, https://doi.org/10.5194/gmd-4-1051-2011, 2011.

Dardel, C., Kergoat, L., Hiernaux, P., Mougin, E., Grippa, M., and Tucker, C. J.: Re-greening Sahel: 30years of remote sensing data and field observations (Mali, Niger), Remote Sens. Environ., 140, 350–364, https://doi.org/10.1016/j.rse.2013.09.011, 2014.

730 Dee, D. P., Uppala, S. M., Simmons, A. J., Berrisford, P., Poli, P., Kobayashi, S., Andrae, U., Balmaseda, M. A., Balsamo, G., Bauer, P., Bechtold, P., Beljaars, A. C. M., van de Berg, L., Bidlot, J., Bormann, N., Delsol, C., Dragani, R., Fuentes, M., Geer, A. J., Haimberger, L., Healy, S. B., Hersbach, H., Hólm, E. V., Isaksen, L., Kållberg, P., Köhler, M., Matricardi, M., McNally, A. P., Monge-Sanz, B. M., Morcrette, J.-J., Park, B.-K., Peubey, C., de Rosnay, P., Tavolato, C., Thépaut, J.-N., and Vitart, F.: The ERA-Interim reanalysis: configuration and performance of the data assimilation system, Q. J. R. Meteorol. Soc.,
735 137, 553–597, https://doi.org/10.1002/qj.828, 2011.

Descroix, L., Mahé, G., Lebel, T., Favreau, G., Galle, S., Gautier, E., Olivry, J.-C., Albergel, J., Amogu, O., Cappelaere, B., Dessouassi, R., Diedhiou, A., Le Breton, E., Mamadou, I., and Sighomnou, D.: Spatio-temporal variability of hydrological regimes around the boundaries between Sahelian and Sudanian areas of West Africa: A synthesis, J. Hydrol., 375, 90–102, https://doi.org/10.1016/j.jhydrol.2008.12.012, 2009.

740 Diene, S. M., Diack, I., Audebert, A., Roupsard, O., Leroux, L., Diouf, A. A., Mbaye, M., Fernandez, R., Diallo, M., and Sarr, I.: Improving pearl millet yield estimation from UAV imagery in the semiarid agroforestry system of Senegal through textural indices and reflectance normalization, IEEE Access, 1–1, https://doi.org/10.1109/ACCESS.2024.3460107, 2024.

Diongue, D. M. L., Roupsard, O., Do, F. C., Stumpp, C., Orange, D., Sow, S., Jourdan, C., and Faye, S.: Evaluation of parameterisation approaches for estimating soil hydraulic parameters with HYDRUS-1D in the groundnut basin of Senegal,
745 Hydrol. Sci. J., 67, 2327–2343, https://doi.org/10.1080/02626667.2022.2142474, 2022.

Diongue, D. M. L., Stumpp, C., Roupsard, O., Orange, D., Do, F. C., and Faye, S.: Estimating water fluxes in the critical zone using water stable isotope approaches in the Groundnut and Ferlo basins of Senegal, Hydrol. Process., 37, e14787, https://doi.org/10.1002/hyp.14787, 2023.

Do, F. C., Goudiaby, V. A., Gimenez, O., Diagne, A. L., Diouf, M., Rocheteau, A., and Akpo, L. E.: Environmental influence
750 on canopy phenology in the dry tropics, For. Ecol. Manag., 215, 319–328, https://doi.org/10.1016/j.foreco.2005.05.022, 2005.

Dosio, A., Jury, M. W., Almazroui, M., Ashfaq, M., Diallo, I., Engelbrecht, F. A., Klutse, N. A. B., Lennard, C., Pinto, I., Sylla, M. B., and Tamoffo, A. T.: Projected future daily characteristics of African precipitation based on global (CMIP5, CMIP6) and regional (CORDEX, CORDEX-CORE) climate models, Clim. Dyn., 57, 3135–3158, https://doi.org/10.1007/s00382-021-05859-w, 2021.

755 Ducharne, A., Ottle, C., Maignan, F., Vuichard, N., Ghattas, J., Wang, F., Peylin, P., Polcher, J., Guimberteau, M., Maugis, P., Tafasca, S., Tootchi, A., Verhoef, A., and Mizuochi, H.: The hydrol module of ORCHIDEE: scientific documentation [rev 3977] and on, work in progress, towards CMIP6v1, Institut Pierre Simon Laplace, Paris, France, 2018.

Eamus, D., Cleverly, J., Boulain, N., Grant, N., Faux, R., and Villalobos-Vega, R.: Carbon and water fluxes in an arid-zone *Acacia* savanna woodland: An analyses of seasonal patterns and responses to rainfall events, Agric. For. Meteorol., 182–183,
760 225–238, https://doi.org/10.1016/j.agrformet.2013.04.020, 2013.

Eldridge, D. J., Ding, J., Dorrough, J., Delgado-Baquerizo, M., Sala, O., Gross, N., Le Bagousse-Pinguet, Y., Mallen-Cooper, M., Saiz, H., Asensio, S., Ochoa, V., Gozalo, B., Guirado, E., García-Gómez, M., Valencia, E., Martínez-Valderrama, J., Plaza, C., Abedi, M., Ahmadian, N., Ahumada, R. J., Alcántara, J. M., Amghar, F., Azevedo, L., Ben Salem, F., Berdugo, M., Blaum, N., Boldgiv, B., Bowker, M., Bran, D., Bu, C., Canessa, R., Castillo-Monroy, A. P., Castro, I., Castro-Quezada, P., Cesarz, S.,
765 Chibani, R., Conceição, A. A., Darrouzet-Nardi, A., Davila, Y. C., Deák, B., Díaz-Martínez, P., Donoso, D. A., Dougill, A. D., Durán, J., Eisenhauer, N., Ejtehadi, H., Espinosa, C. I., Fajardo, A., Farzam, M., Foronda, A., Franzese, J., Fraser, L. H., Gaitán, J., Geissler, K., Gonzalez, S. L., Gusman-Montalvan, E., Hernández, R. M., Hölzel, N., Hughes, F. M., Jadan, O., Jentsch, A., Ju, M., Kaseke, K. F., Köbel, M., Lehmann, A., Liancourt, P., Linstädter, A., Louw, M. A., Ma, Q., Mabaso, M., Maggs-Kölling, G., Makhalanyane, T. P., Issa, O. M., Marais, E., McClaran, M., Mendoza, B., Mokoka, V., Mora, J. P.,
770 Moreno, G., Munson, S., Nunes, A., Oliva, G., Oñatibia, G. R., Osborne, B., Peter, G., Pierre, M., Pueyo, Y., Emiliano Quiroga, R., Reed, S., Rey, A., Rey, P., Gómez, V. M. R., Rolo, V., Rillig, M. C., le Roux, P. C., Ruppert, J. C., Salah, A., Sebei, P. J., Sharkhuu, A., et al.: Hotspots of biogeochemical activity linked to aridity and plant traits across global drylands, Nat. Plants, 10, 760–770, https://doi.org/10.1038/s41477-024-01670-7, 2024.

Farquhar, G. D., von Caemmerer, S., and Berry, J. A.: A biochemical model of photosynthetic $CO_2$ assimilation in leaves of
775 C3 species, Planta, 149, 78–90, https://doi.org/10.1007/BF00386231, 1980.

Favreau, G., Cappelaere, B., Massuel, S., Leblanc, M., Boucher, M., Boulain, N., and Leduc, C.: Land clearing, climate variability, and water resources increase in semiarid southwest Niger: A review, Water Resour. Res., 45, https://doi.org/10.1029/2007WR006785, 2009.

Fawcett, D., Cunliffe, A. M., Sitch, S., O'Sullivan, M., Anderson, K., Brazier, R. E., Hill, T. C., Anthoni, P., Arneth, A., Arora,
780 V. K., Briggs, P. R., Goll, D. S., Jain, A. K., Li, X., Lombardozzi, D., Nabel, J. E. M. S., Poulter, B., Séférian, R., Tian, H., Viovy, N., Wigneron, J.-P., Wiltshire, A., and Zaehle, S.: Assessing Model Predictions of Carbon Dynamics in Global Drylands, Front. Environ. Sci., 10, https://doi.org/10.3389/fenvs.2022.790200, 2022.

Faye, B., Webber, H., Diop, M., Mbaye, M. L., Owusu-Sekyere, J. D., Naab, J. B., and Gaiser, T.: Potential impact of climate change on peanut yield in Senegal, West Africa, Field Crops Res., 219, 148–159, https://doi.org/10.1016/j.fcr.2018.01.034,
785 2018.

Fensholt, R., Rasmussen, K., Kaspersen, P., Huber, S., Horion, S., and Swinnen, E.: Assessing Land Degradation/Recovery in the African Sahel from Long-Term Earth Observation Based Primary Productivity and Precipitation Relationships, Remote Sens., 5, 664–686, https://doi.org/10.3390/rs5020664, 2013.

Finkelstein, P. L. and Sims, P. F.: Sampling error in eddy correlation flux measurements, J. Geophys. Res. Atmospheres, 106,
790 3503–3509, https://doi.org/10.1029/2000JD900731, 2001.

Foken, T., Göockede, M., Mauder, M., Mahrt, L., Amiro, B., and Munger, W.: Post-Field Data Quality Control, in: Handbook of Micrometeorology: A Guide for Surface Flux Measurement and Analysis, edited by: Lee, X., Massman, W., and Law, B., Springer Netherlands, Dordrecht, 181–208, https://doi.org/10.1007/1-4020-2265-4_9, 2005.

795 Gaglo, K. E., Valade, A., and Roupsard, O.: Data and code for GMD paper: Sensitivity of a Sahelian groundwater-based agroforestry system to tree density and water availability using the land surface model ORCHIDEE (r7949), https://doi.org/10.5281/zenodo.15383628, 2025a.

Gaglo, K. E., Chaste, E., and Valade, A.: ORCHIDEE r7949, https://doi.org/10.5281/zenodo.15313734, 2025b.

Glanville, K., Sheldon, F., Butler, D., and Capon, S.: Effects and significance of groundwater for vegetation: A systematic review, Sci. Total Environ., 875, 162577, https://doi.org/10.1016/j.scitotenv.2023.162577, 2023.

800 Gning, F., Jourdan, C., Marone, D., Ngom, D., and Ræbild, A.: Root distribution of Adansonia digitata, Faidherbia albida and Borassus akeassii along a climate gradient in Senegal, Agrofor. Syst., 97, 605–615, https://doi.org/10.1007/s10457-023-00813-7, 2023.

Harris, I., Osborn, T. J., Jones, P., and Lister, D.: Version 4 of the CRU TS monthly high-resolution gridded multivariate climate dataset, Sci. Data, 7, 109, https://doi.org/10.1038/s41597-020-0453-3, 2020.

805 Hedayetullah, M. and Zaman, P.: Forage Crops of the World, 2-volume set: Volume I: Major Forage Crops; Volume II: Minor Forage Crops, CRC Press, 799 pp., 2022.

Herrmann, S. M., Anyamba, A., and Tucker, C. J.: Recent trends in vegetation dynamics in the African Sahel and their relationship to climate, Glob. Environ. Change, 15, 394–404, https://doi.org/10.1016/j.gloenvcha.2005.08.004, 2005.

Huber, S., Fensholt, R., and Rasmussen, K.: Water availability as the driver of vegetation dynamics in the African Sahel from 810 1982 to 2007, Glob. Planet. Change, 76, 186–195, https://doi.org/10.1016/j.gloplacha.2011.01.006, 2011.

Kajuna, S.: Millet: post-harvested operations, edited by: Meija, D. and Beverly, L., Sokone University of Agriculture, 2021.

Kattge, J. and Knorr, W.: Temperature acclimation in a biochemical model of photosynthesis: a reanalysis of data from 36 species, Plant Cell Environ., 30, 1176–1190, https://doi.org/10.1111/j.1365-3040.2007.01690.x, 2007.

Kobayashi, S., Ota, Y., Harada, Y., Ebita, A., Moriya, M., Onoda, H., Onogi, K., Kamahori, H., Kobayashi, C., Endo, H., 815 Miyaoka, K., and Takahashi, K.: The JRA-55 Reanalysis: General Specifications and Basic Characteristics, J. Meteorol. Soc. Jpn. Ser II, 93, 5–48, https://doi.org/10.2151/jmsj.2015-001, 2015.

Kormann, R. and Meixner, F. X.: An Analytical Footprint Model For Non-Neutral Stratification, Bound.-Layer Meteorol., 99, 207–224, https://doi.org/10.1023/A:1018991015119, 2001.

Kotchoni, D. O. V., Vouillamoz, J.-M., Lawson, F. M. A., Adjomayi, P., Boukari, M., and Taylor, R. G.: Relationships between 820 rainfall and groundwater recharge in seasonally humid Benin: a comparative analysis of long-term hydrographs in sedimentary and crystalline aquifers, Hydrogeol. J., 27, 447–457, https://doi.org/10.1007/s10040-018-1806-2, 2019.

Krinner, G., Viovy, N., de Noblet-Ducoudré, N., Ogée, J., Polcher, J., Friedlingstein, P., Ciais, P., Sitch, S., and Prentice, I. C.: A dynamic global vegetation model for studies of the coupled atmosphere-biosphere system, Glob. Biogeochem. Cycles, 19, https://doi.org/10.1029/2003gb002199, 2005.

825    Kumi, N. and Abiodun, B. J.: Potential impacts of 1.5 °C and 2 °C global warming on rainfall onset, cessation and length of rainy season in West Africa, Environ. Res. Lett., 13, 055009, https://doi.org/10.1088/1748-9326/aab89e, 2018.

Lasslop, G., Reichstein, M., Papale, D., Richardson, A. D., Arneth, A., Barr, A., Stoy, P., and Wohlfahrt, G.: Separation of net ecosystem exchange into assimilation and respiration using a light response curve approach: critical issues and global evaluation, Glob. Change Biol., 16, 187–208, https://doi.org/10.1111/j.1365-2486.2009.02041.x, 2010.

830    Lawrence, D. M., Fisher, R. A., Koven, C. D., Oleson, K. W., Swenson, S. C., Bonan, G., Collier, N., Ghimire, B., van Kampenhout, L., Kennedy, D., Kluzek, E., Lawrence, P. J., Li, F., Li, H., Lombardozzi, D., Riley, W. J., Sacks, W. J., Shi, M., Vertenstein, M., Wieder, W. R., Xu, C., Ali, A. A., Badger, A. M., Bisht, G., van den Broeke, M., Brunke, M. A., Burns, S. P., Buzan, J., Clark, M., Craig, A., Dahlin, K., Drewniak, B., Fisher, J. B., Flanner, M., Fox, A. M., Gentine, P., Hoffman, F., Keppel-Aleks, G., Knox, R., Kumar, S., Lenaerts, J., Leung, L. R., Lipscomb, W. H., Lu, Y., Pandey, A., Pelletier, J. D.,
835    Perket, J., Randerson, J. T., Ricciuto, D. M., Sanderson, B. M., Slater, A., Subin, Z. M., Tang, J., Thomas, R. Q., Val Martin, M., and Zeng, X.: The Community Land Model Version 5: Description of New Features, Benchmarking, and Impact of Forcing Uncertainty, J. Adv. Model. Earth Syst., 11, 4245–4287, https://doi.org/10.1029/2018MS001583, 2019.

Leduc, C., Favreau, G., and Schroeter, P.: Long-term rise in a Sahelian water-table: the Continental Terminal in South-West Niger, J. Hydrol., 243, 43–54, https://doi.org/10.1016/S0022-1694(00)00403-0, 2001.

840    Lericollais, A.: Sob: étude géographique d'un terroir sérèr (Sénégal), IRD Editions, 134 pp., 1972.

Lericollais, A.: La dégradation de l'aménagement agraire, in: Paysans sereer : Dynamiques agraires et mobilités au Sénégal, IRD Éditions, Marseille, 117–138, https://doi.org/10.4000/books.irdeditions.15915, 1999.

Levins, R.: The Strategy of Model Building in Population Biology, Am. Sci., 54, 421–431, 1966.

Li, D., Malyshev, S., and Shevliakova, E.: Exploring historical and future urban climate in the Earth System Modeling
845    framework: 1. Model development and evaluation, J. Adv. Model. Earth Syst., 8, 917–935, https://doi.org/10.1002/2015MS000578, 2016.

Li-Cor, I.: LAI-2200 Plant Canopy Analyzer: Instruction manual, 2012.

MacBean, N., Maignan, F., Peylin, P., Bacour, C., Bréon, F.-M., and Ciais, P.: Using satellite data to improve the leaf phenology of a global terrestrial biosphere model, Biogeosciences, 12, 7185–7208, https://doi.org/10.5194/bg-12-7185-2015,
850    2015.

MacBean, N., Scott, R. L., Biederman, J. A., Peylin, P., Kolb, T., Litvak, M. E., Krishnan, P., Meyers, T. P., Arora, V. K., Bastrikov, V., Goll, D., Lombardozzi, D. L., Nabel, J. E. M. S., Pongratz, J., Sitch, S., Walker, A. P., Zaehle, S., and Moore, D. J. P.: Dynamic global vegetation models underestimate net $CO_2$ flux mean and inter-annual variability in dryland ecosystems, Environ. Res. Lett., 16, 094023, https://doi.org/10.1088/1748-9326/ac1a38, 2021.

855    Madani, N., Kimball, J. S., Parazoo, N. C., Ballantyne, A. P., Tagesson, T., Jones, L. A., Reichle, R. H., Palmer, P. I., Velicogna, I., Bloom, A. A., Saatchi, S., Liu, Z., and Geruo, A.: Below-surface water mediates the response of African forests to reduced rainfall, Environ. Res. Lett., 15, 034063, https://doi.org/10.1088/1748-9326/ab724a, 2020.

Mahnken, M., Cailleret, M., Collalti, A., Trotta, C., Biondo, C., D'Andrea, E., Dalmonech, D., Marano, G., Mäkelä, A., Minunno, F., Peltoniemi, M., Trotsiuk, V., Nadal-Sala, D., Sabaté, S., Vallet, P., Aussenac, R., Cameron, D. R., Bohn, F. J.,
860    Grote, R., Augustynczik, A. L. D., Yousefpour, R., Huber, N., Bugmann, H., Merganičová, K., Merganic, J., Valent, P., Lasch-Born, P., Hartig, F., Vega del Valle, I. D., Volkholz, J., Gutsch, M., Matteucci, G., Krejza, J., Ibrom, A., Meesenburg, H.,

34

Rötzer, T., van der Maaten-Theunissen, M., van der Maaten, E., and Reyer, C. P. O.: Accuracy, realism and general applicability of European forest models, Glob. Change Biol., 28, 6921–6943, https://doi.org/10.1111/gcb.16384, 2022.

865 Marteau, R., Sultan, B., Moron, V., Alhassane, A., Baron, C., and Traoré, S. B.: The onset of the rainy season and farmers' sowing strategy for pearl millet cultivation in Southwest Niger, Agric. For. Meteorol., 151, 1356–1369, https://doi.org/10.1016/j.agrformet.2011.05.018, 2011.

Maslin, B., Miller, J., and Seigler, D.: Overview of the generic status of Acacia (Leguminosae: Mimosoideae), Aust. Syst. Bot. - AUST Syst. Bot., 16, https://doi.org/10.1071/SB02008, 2003.

Medlyn, B. E., Dreyer, E., Ellsworth, D., Forstreuter, M., Harley, P. C., Kirschbaum, M. U. F., Le Roux, X., Montpied, P.,
870 Strassemeyer, J., Walcroft, A., Wang, K., and Loustau, D.: Temperature response of parameters of a biochemically based model of photosynthesis. II. A review of experimental data, Plant Cell Environ., 25, 1167–1179, https://doi.org/10.1046/j.1365-3040.2002.00891.x, 2002.

Meinshausen, M., Schleussner, C.-F., Beyer, K., Bodeker, G., Boucher, O., Canadell, J. G., Daniel, J. S., Diongue-Niang, A., Driouech, F., Fischer, E., Forster, P., Grose, M., Hansen, G., Hausfather, Z., Ilyina, T., Kikstra, J. S., Kimutai, J., King, A. D.,
875 Lee, J.-Y., Lennard, C., Lissner, T., Nauels, A., Peters, G. P., Pirani, A., Plattner, G.-K., Pörtner, H., Rogelj, J., Rojas, M., Roy, J., Samset, B. H., Sanderson, B. M., Séférian, R., Seneviratne, S., Smith, C. J., Szopa, S., Thomas, A., Urge-Vorsatz, D., Velders, G. J. M., Yokohata, T., Ziehn, T., and Nicholls, Z.: A perspective on the next generation of Earth system model scenarios: towards representative emission pathways (REPs), Geosci. Model Dev., 17, 4533–4559, https://doi.org/10.5194/gmd-17-4533-2024, 2024.

880 Moncrieff, J., Clement, R., Finnigan, J., and Meyers, T.: Averaging, Detrending, and Filtering of Eddy Covariance Time Series, in: Handbook of Micrometeorology: A Guide for Surface Flux Measurement and Analysis, edited by: Lee, X., Massman, W., and Law, B., Springer Netherlands, Dordrecht, 7–31, https://doi.org/10.1007/1-4020-2265-4_2, 2005.

Moncrieff, J. B., Massheder, J. M., de Bruin, H., Elbers, J., Friborg, T., Heusinkveld, B., Kabat, P., Scott, S., Soegaard, H., and Verhoef, A.: A system to measure surface fluxes of momentum, sensible heat, water vapour and carbon dioxide, J. Hydrol.,
885 188–189, 589–611, https://doi.org/10.1016/S0022-1694(96)03194-0, 1997.

Murphy, P. G. and Lugo, A. E.: Ecology of tropical dry forest, Annu. Rev. Ecol. Evol. Syst., 17, 67–88, https://doi.org/10.1146/annurev.es.17.110186.000435, 1986.

Ndehedehe, C., Awange, J., Agutu, N., Kuhn, M., and Heck, B.: Understanding changes in terrestrial water storage over West Africa between 2002 and 2014, Adv. Water Resour., 88, 211–230, https://doi.org/10.1016/j.advwatres.2015.12.009, 2016.

890 Ndehedehe, C. E., Ferreira, V. G., and Agutu, N. O.: Hydrological controls on surface vegetation dynamics over West and Central Africa, Ecol. Indic., 103, 494–508, https://doi.org/10.1016/j.ecolind.2019.04.032, 2019.

Ndiaye, M. B., Sine, B., Sambakhe, D., Diallo, A. O., Muller, B., Sene, M., and Sambou, S.: Characterization of the starting conditions of the rainy season in Senegal: highlighting the constraints of crop establishment, Environ. Res. Commun., 6, 075024, https://doi.org/10.1088/2515-7620/ad5081, 2024.

895 Ntare, B. R., Diallo, A. T., Ndjeunga, J., and Waliyar, F.: Groundnut Seed production Manual, International Crops Research Institute for the Semi-Arid Tropics (ICRISAT), Patancheru 502 324, Andhra Pradesh, India, 20 pp., 2008.

Palmer, P. I., Wainwright, C. M., Dong, B., Maidment, R. I., Wheeler, K. G., Gedney, N., Hickman, J. E., Madani, N., Folwell, S. S., Abdo, G., Allan, R. P., Black, E. C. L., Feng, L., Gudoshava, M., Haines, K., Huntingford, C., Kilavi, M., Lunt, M. F.,

Shaaban, A., and Turner, A. G.: Drivers and impacts of Eastern African rainfall variability, Nat. Rev. Earth Environ., 4, 254–270, https://doi.org/10.1038/s43017-023-00397-x, 2023.

Pélissier, P.: Les Paysans du Sénégal: les civilisations agraires du Cayor à la Casamance ..., Impr. Fabrègue, 1034 pp., 1966.

Pontailler, J.-Y., Hymus, G. J., and Drake, B. G.: Estimation of leaf area index using ground-based remote sensed NDVI measurements: validation and comparison with two indirect techniques, Can. J. Remote Sens., 29, 381–387, https://doi.org/10.5589/m03-009, 2003.

Poulter, B., MacBean, N., Hartley, A., Khlystova, I., Arino, O., Betts, R., Bontemps, S., Boettcher, M., Brockmann, C., Defourny, P., Hagemann, S., Herold, M., Kirches, G., Lamarche, C., Lederer, D., Ottle, C., Peters, M., and Peylin, P.: Plant functional type classification for earth system models: results from the European Space Agency's Land Cover Climate Change Initiative, Geosci. Model Dev., 8, 2315–2328, https://doi.org/10.5194/gmd-8-2315-2015, 2015.

R Core Team: R: A Language and Environment for Statistical Computing, 2024.

Rahimi, J., Ago, E. E., Ayantunde, A., Berger, S., Bogaert, J., Butterbach-Bahl, K., Cappelaere, B., Cohard, J. M., Demarty, J., Diouf, A. A., Falk, U., Haas, E., Hiernaux, P., Kraus, D., Roupsard, O., Scheer, C., Srivastava, A. K., Tagesson, T., and Grote, R.: Modeling gas exchange and biomass production in West African Sahelian and Sudanian ecological zones, Geosci. Model Dev., 14, 3789–3812, https://doi.org/10.5194/gmd-14-3789-2021, 2021.

Reichstein, M., Bahn, M., Ciais, P., Frank, D., Mahecha, M. D., Seneviratne, S. I., Zscheischler, J., Beer, C., Buchmann, N., Frank, D. C., Papale, D., Rammig, A., Smith, P., Thonicke, K., van der Velde, M., Vicca, S., Walz, A., and Wattenbach, M.: Climate extremes and the carbon cycle, Nature, 500, 287–295, https://doi.org/10.1038/nature12350, 2013.

de Rosnay, P., Polcher, J., Bruen, M., and Laval, K.: Impact of a physically based soil water flow and soil-plant interaction representation for modeling large-scale land surface processes, J. Geophys. Res. Atmospheres, 107, ACL 3-1-ACL 3-19, https://doi.org/10.1029/2001jd000634, 2002.

Roupsard, O., Ferhi, A., Granier, A., Pallo, F., Depommier, D., Mallet, B., Joly, H. I., and Dreyer, E.: Reverse phenology and dry-season water uptake by Faidherbia albida (Del.) A. Chev. in an agroforestry parkland of Sudanese west Africa, Funct. Ecol., 13, 460–472, https://doi.org/10.1046/j.1365-2435.1999.00345.x, 1999.

Roupsard, O., Audebert, A., Ndour, A. P., Clermont-Dauphin, C., Agbohessou, Y., Sanou, J., Koala, J., Faye, E., Sambakhe, D., Jourdan, C., le Maire, G., Tall, L., Sanogo, D., Seghieri, J., Cournac, L., and Leroux, L.: How far does the tree affect the crop in agroforestry? New spatial analysis methods in a Faidherbia parkland, Agric. Ecosyst. Environ., 296, https://doi.org/10.1016/j.agee.2020.106928, 2020.

Roupsard, O., Faye, W., Sow, S., Diongue, D. M. L., Orange, D., Do, F. C., Jourdan, C., Stumpp, C., and Faye, S.: Inverted phenology of #Faidherbia albida# paced with the dynamics of the water table, Congrès mondial d'agroforesterie, public, 5, 1 p., 2022.

Sanon, M., Hoogenboom, G., Traoré, S. B., Sarr, B., Garcia, A. G. y, Somé, L., and Roncoli, C.: Photoperiod sensitivity of local millet and sorghum varieties in West Africa, NJAS - Wagening. J. Life Sci., 68, 29–39, https://doi.org/10.1016/j.njas.2013.11.004, 2014.

Sarr, M. S., Diouf, K., Roupsard, O., Rocheteau, A., Orange, D., Jourdan, C., Diehdiou, I., Seghieri, J., and C. Do, F.: Estimation of seasonal water use of Faidherbia albida (Delile) A.Chev. in a Sahelian agroforestry parkland, BASE, 2023.

935   Scanlon, B. R., Reedy, R. C., Stonestrom, D. A., Prudic, D. E., and Dennehy, K. F.: Impact of land use and land cover change on groundwater recharge and quality in the southwestern US, Glob. Change Biol., 11, 1577–1593, https://doi.org/10.1111/j.1365-2486.2005.01026.x, 2005.

Scanlon, B. R., Keese, K. E., Flint, A. L., Flint, L. E., Gaye, C. B., Edmunds, W. M., and Simmers, I.: Global synthesis of groundwater recharge in semiarid and arid regions, Hydrol. Process., 20, 3335–3370, https://doi.org/10.1002/hyp.6335, 2006.

940   Seghieri, J., Vescovo, A., Padel, K., Soubie, R., Arjounin, M., Boulain, N., de Rosnay, P., Galle, S., Gosset, M., Mouctar, A. H., Peugeot, C., and Timouk, F.: Relationships between climate, soil moisture and phenology of the woody cover in two sites located along the West African latitudinal gradient, J. Hydrol., 375, 78–89, https://doi.org/10.1016/j.jhydrol.2009.01.023, 2009.

Siegwart, L., Bertrand, I., Roupsard, O., Duthoit, M., and Jourdan, C.: Root litter decomposition in a sub-Sahelian agroforestry
945   parkland dominated by Faidherbia albida, J. Arid Environ., 198, 104696, https://doi.org/10.1016/j.jaridenv.2021.104696, 2022.

Siegwart, L., Bertrand, I., Roupsard, O., and Jourdan, C.: Contribution of tree and crop roots to soil carbon stocks in a Sub-Sahelian agroforestry parkland in Senegal, Agric. Ecosyst. Environ., 352, 108524, https://doi.org/10.1016/j.agee.2023.108524, 2023.

950   Sileshi, G. W.: The magnitude and spatial extent of influence of Faidherbia albida trees on soil properties and primary productivity in drylands, J. Arid Environ., 132, 1–14, https://doi.org/10.1016/j.jaridenv.2016.03.002, 2016.

Soudani, K., Hmimina, G., Delpierre, N., Pontailler, J.-Y., Aubinet, M., Bonal, D., Caquet, B., de Grandcourt, A., Burban, B., Flechard, C., Guyon, D., Granier, A., Gross, P., Heinesh, B., Longdoz, B., Loustau, D., Moureaux, C., Ourcival, J.-M., Rambal, S., Saint André, L., and Dufrêne, E.: Ground-based Network of NDVI measurements for tracking temporal dynamics of canopy
955   structure and vegetation phenology in different biomes, Remote Sens. Environ., 123, 234–245, https://doi.org/10.1016/j.rse.2012.03.012, 2012.

Sow, S., Senghor, Y., Sadio, K., Vezy, R., Roupsard, O., Affholder, F., N'dienor, M., Clermont-Dauphin, C., Gaglo, E. K., Ba, S., Tounkara, A., Balde, A. B., Agbohessou, Y., Seghieri, J., Sall, S. N., Couedel, A., Leroux, L., Jourdan, C., Diaite, D. S., and Falconnier, G. N.: Calibrating the STICS soil-crop model to explore the impact of agroforestry parklands on millet
960   growth, Field Crops Res., 306, 109206, https://doi.org/10.1016/j.fcr.2023.109206, 2024.

Taugourdeau, S., le Maire, G., Avelino, J., Jones, J. R., Ramirez, L. G., Jara Quesada, M., Charbonnier, F., Gómez-Delgado, F., Harmand, J.-M., Rapidel, B., Vaast, P., and Roupsard, O.: Leaf area index as an indicator of ecosystem services and management practices: An application for coffee agroforestry, Agric. Ecosyst. Environ., 192, 19–37, https://doi.org/10.1016/j.agee.2014.03.042, 2014.

965   Toure, A., Diekkrüger, B., and Mariko, A.: Impact of Climate Change on Groundwater Resources in the Klela Basin, Southern Mali, Hydrology, 3, 17, https://doi.org/10.3390/hydrology3020017, 2016.

Tovignan, T. K., Fonceka, D., Ndoye, I., Cisse, N., and Luquet, D.: The sowing date and post-flowering water status affect the sugar and grain production of photoperiodic, sweet sorghum through the regulation of sink size and leaf area dynamics, Field Crops Res., 192, 67–77, https://doi.org/10.1016/j.fcr.2016.04.015, 2016.

970   Vandenbeldt, R. J., International Crops Research Institute for the Semi-arid Tropics, and International Centre for Research in Agroforestry (Eds.): Faidherbia albida in the west African semi-arid tropics: proceedings of a workshop, 22-26 Apr. 1991, Niamey, Niger, International Crops Research Institute for the Semi-arid Tropics ; International Centre for Research in Agroforestry, Patancheru, Andhra Pradesh, India : Nairobi, Kenya, 206 pp., 1992.

Vandewalle, N.: Paramétrisation de la photosynthèse foliaire de Faidherbia albida au sein d'un parc agroforestier dans le bassin arachidier du Sénégal, Université Catholique de Louvain, Louvain-la-Neuve, Belgium, 106 pp., 2024.

Vickers, D. and Mahrt, L.: Quality Control and Flux Sampling Problems for Tower and Aircraft Data, 1997.

Vuichard, N. and Papale, D.: Filling the gaps in meteorological continuous data measured at FLUXNET sites with ERA-Interim reanalysis, Earth Syst. Sci. Data, 7, 157–171, https://doi.org/10.5194/essd-7-157-2015, 2015.

Vuichard, N., Messina, P., Luyssaert, S., Guenet, B., Zaehle, S., Ghattas, J., Bastrikov, V., and Peylin, P.: Accounting for carbon and nitrogen interactions in the global terrestrial ecosystem model ORCHIDEE (trunk version, rev 4999): multi-scale evaluation of gross primary production, Geosci. Model Dev., 12, 4751–4779, https://doi.org/10.5194/gmd-12-4751-2019, 2019.

Wang, S., Zhang, Y., Ju, W., Chen, J. M., Ciais, P., Cescatti, A., Sardans, J., Janssens, I. A., Wu, M., Berry, J. A., Campbell, E., Fernandez-Martinez, M., Alkama, R., Sitch, S., Friedlingstein, P., Smith, W. K., Yuan, W., He, W., Lombardozzi, D., Kautz, M., Zhu, D., Lienert, S., Kato, E., Poulter, B., Sanders, T. G. M., Kruger, I., Wang, R., Zeng, N., Tian, H., Vuichard, N., Jain, A. K., Wiltshire, A., Haverd, V., Goll, D. S., and Penuelas, J.: Recent global decline of CO2 fertilization effects on vegetation photosynthesis, Science, 370, 1295–1300, https://doi.org/10.1126/science.abb7772, 2020.

Webb, E. K., Pearman, G. I., and Leuning, R.: Correction of flux measurements for density effects due to heat and water vapour transfer, Q. J. R. Meteorol. Soc., 106, 85–100, https://doi.org/10.1002/qj.49710644707, 1980.

Wickens, G. E.: A Study of Acacia albida Del. (Mimosoïdeae), Kew Bull., 23, 181–202, https://doi.org/10.2307/4108947, 1969.

Williams, I. N. and Torn, M. S.: Vegetation controls on surface heat flux partitioning, and land-atmosphere coupling, Geophys. Res. Lett., 42, 9416–9424, https://doi.org/10.1002/2015GL066305, 2015.

Wutzler, T., Lucas-Moffat, A., Migliavacca, M., Knauer, J., Sickel, K., Šigut, L., Menzer, O., and Reichstein, M.: Basic and extensible post-processing of eddy covariance flux data with REddyProc, Biogeosciences, 15, 5015–5030, https://doi.org/10.5194/bg-15-5015-2018, 2018.

Xenakis, G.: FREddyPro: post-processing EddyPro full output file, 2016.

Yin, L., Zhou, Y., Huang, J., Wenninger, J., Zhang, E., Hou, G., and Dong, J.: Interaction between groundwater and trees in an arid site: Potential impacts of climate variation and groundwater abstraction on trees, J. Hydrol., 528, 435–448, https://doi.org/10.1016/j.jhydrol.2015.06.063, 2015.

Yin, X. and Struik, P. C.: C3 and C4 photosynthesis models: An overview from the perspective of crop modelling, NJAS - Wagening. J. Life Sci., 57, 27–38, https://doi.org/10.1016/j.njas.2009.07.001, 2009.

Zhang, W., Brandt, M., Tong, X., Tian, Q., and Fensholt, R.: Impacts of the seasonal distribution of rainfall on vegetation productivity across the Sahel, Biogeosciences, 15, 319–330, https://doi.org/10.5194/bg-15-319-2018, 2018.